

LLAMP: LARGE LANGUAGE MODEL MADE POWERFUL FOR HIGH-FIDELITY MATERIALS KNOWLEDGE RETRIEVAL

Anonymous authors

Paper under double-blind review

ABSTRACT

Reducing hallucination of Large Language Models (LLMs) is imperative for use in the sciences, where reliability and reproducibility are crucial. However, LLMs inherently lack long-term memory, making it a nontrivial, *ad hoc*, and often biased task to fine-tune them on domain-specific literature and data. Here we introduce **LLaMP**, a multimodal retrieval-augmented generation (RAG) framework of hierarchical reasoning-and-acting (ReAct) agents that can dynamically and recursively interact with computational and experimental data from the [Materials Project \(MP\)](#) and run atomistic simulations via high-throughput workflow interface. Without fine-tuning, LLaMP demonstrates strong tool-usage ability to comprehend and integrate various modalities of materials science concepts, fetch relevant data stores on the fly, process higher-order data (such as crystal structure and elastic tensor), and streamline complex tasks in computational materials and chemistry. We propose a metric combining uncertainty and confidence estimates to evaluate the self-consistency of responses by LLaMP and vanilla LLMs. Our benchmark shows that LLaMP effectively mitigates the intrinsic bias in LLMs, counteracting the errors on bulk moduli, electronic bandgaps, and formation energies that seem to derive from mixed data sources. We also demonstrate LLaMP’s capability to edit crystal structures and run annealing molecular dynamics simulations using pre-trained machine-learning interatomic potentials. The framework offers an intuitive and nearly hallucination-free approach to exploring and scaling materials informatics, and paves the way for future agentic scientific workflows and knowledge-grounded LLMs.

1 INTRODUCTION

The generation of convincing yet unreliable information poses a pressing challenge to large language model (LLMs), particularly to their application in the sciences. LLMs are prone to hallucination—providing outright false information with high confidence (Bang et al., 2023; Xu et al., 2024). This issue is particularly concerning for knowledge-intensive tasks, where users rely on chatbots and other AI systems to provide accurate guidance (Lewis et al., 2020). LLMs often lack up-to-date factual knowledge on topics outside their training data, requiring rigorous verification against trusted external sources (Mallen et al., 2023). In the scientific community, where the integration of insights and data accuracy is already complex, the proliferation of generative models may exacerbate the risk of misinformation. This trend accentuates the importance of scrutinizing and ensuring the reliability of information sources.

Current approaches to enhance LLM accuracy in domain-specific knowledge often involve fine-tuning pre-trained models (Dagdelen et al., 2024; Gupta et al., 2022) or tailored prompt engineering techniques (Yang et al., 2023; Zheng et al., 2023). While these models are easy to deploy, they suffer from diminished reproducibility and data adherence due to the absence of a memory base, untraceable fine-tuning history, or opaque extraction processes. Even though fine-tuning can encode a certain amount of domain-specific knowledge into LLMs, it is constrained by scalability and intrinsic memory capacity. Fine-tuned LLMs struggle to retain in the long term the knowledge they were trained on as the training progresses, nor can they be aware of the recent events and data beyond pre-training. Prompt engineering, while effective, also compromises the generalizability, thus limiting

054 the overall power and flexibility of LLMs. Therefore, a more sensible approach involves equipping
055 LLMs with external data sources, allowing them to generate holistic responses via few-shot adapta-
056 tion to factual information (Lewis et al., 2021) that can reliably support real-world scientific research
057 and decision-making.

058 In this work, we propose LLaMP, a multimodal retrieval-augmented generation (RAG) framework
059 leveraging hierarchical reasoning-and-acting (ReAct) agents to interact with Materials Project (MP),
060 arXiv, Wikipedia, and atomistic simulation tools. The framework serves as a safeguard against
061 LLM hallucination by grounding them in high-fidelity material informatics ~~from large-scale mate-
062 rial databasederived from various sources~~, including ~~computational data from~~ quantum-mechanical
063 first-principles calculations and expert-curated material synthesis recipes, and further enables the
064 capabilities of complex downstream tasks. ~~The hierarchical planning of supervisor and assistant
065 ReAct agents improves self-correcting tool-usage performance and enhances the self-consistency
066 in final responses. The new capabilities emerge—such as multi-modal searching, tensor and 3D
067 crystal structure retrieval and operation, and language-driven simulation. The frameworkThrough
068 hierarehical planning of multiple ReAct agents, we demonstrate that LLaMP~~ not only can correctly
069 retrieve ~~high-fidelity, higher-order materials datahigher-order materials data such as tensors and
070 3D-crystal-structures~~ but also can combine different modalities to perform complex, knowledge-
071 intensive inferences and operations essential for real-world materials science applications.

072 Our contributions are as follows: (1) we introduce a multimodal RAG framework employing hierar-
073 chical ReAct agents that dynamically interact with the Materials Project, enabling LLMs to access
074 high-fidelity materials informatics; (2) we propose a statistical metric to assess the self-consistency
075 of LLM responses in high-precision, reproducibility-critical settings; (3) we evaluate the perfor-
076 mance of LLaMP and standard LLMs in predicting key material properties, including bulk moduli,
077 electronic bandgaps, formation energies, and magnetic orderings; (4) we showcase real-world appli-
078 cations in materials science, such as inorganic synthesis and crystal structure generation and editing;
079 (5) we enhance LLaMP with high-throughput atomistic simulation workflows and pre-trained uni-
080 versal ML force fields, lowering the entry barriers to computational materials and chemistry.

081 2 BACKGROUND

082 **Materials Project (MP)** The Materials Project is a multi-institution effort to explore and com-
083 pute the properties of all known inorganic materials (Jain et al., 2013) and molecules (Spotte-Smith
084 et al., 2023). The initiative leverages high-throughput electronic structure calculations (Kresse and
085 Furthmüller, 1996; Shao et al., 2015) based on density functional theory (DFT), providing large-
086 scale open-source database and analysis algorithms, with the ultimate goal to drastically reduce the
087 time and cost required for materials discovery by focusing experiments on the promising candidates
088 from computational screening. Most of the atomic structures are selected from the Inorganic Crystal
089 Structure Database (ICSD) (Zagorac et al., 2019) and undergo standardized relaxation procedures,
090 followed by post-processing or additional calculations for higher-order material properties such as
091 electron and phonon bandgaps, elastic tensors, dielectric tensors, and more. MP provides these
092 calculated material properties through API endpoints.

093 **NLP and LLM in materials science** Natural language processing (NLP) has found extensive
094 application in extracting valuable information from scientific publications, with notable instances
095 involving text-to-text or more recent image-to-text summarization techniques (Gupta et al., 2022;
096 Radford et al., 2021; Tshitoyan et al., 2019). For summarizing crystal structures in textual form,
097 Ganose and Jain (2019) introduced the *robocrystallographer*, a toolkit designed for the analysis
098 and generation of descriptions for crystalline materials. Their method condenses atomic structures
099 into descriptive JSON representations that encompass coordination statistics, connectivity motifs,
100 geometric features, and dimensionality. MP leverages robocrystallographer to generate human-level
101 descriptions for 130K compounds which are accessible through MP website and API.

102 ~~Recent efforts have curated datasets (Zaki et al., 2023) and benchmarks (Song et al., 2023) to better
103 evaluate the limitations of LLMs in question answering within the materials science domain. Zhang
104 et al. (2024) further curated instruction data to fine-tune Llama for material science-specific tasks.
105 These works focus on general (undergraduate-level) question answering instead of factual grounding
106 on expert-curated database and downstream agentic workflow. In a complementary aspect, other
107~~

works address the challenges of extracting complex materials informatics from diverse formats such as tables and unstructured texts (Hira et al., 2024; Schilling-Wilhelmi et al., 2024). This motivates us to augment LLM’s knowledge base with MP—one of the most authoritative materials database of stable crystal structures, high-fidelity DFT calculations, inorganic solid-state synthesis recipes, etc.

3 RELATED WORK

Prompting and fine-tuning in domain science Prompt-based methods have been used as effective tools for automating data extraction process from the literature. Polak and Morgan (2023) employ a prompt workflow to extract the cooling rates of metallic glasses and yield strengths of high entropy alloys. Zheng et al. (2023) implement a ChatGPT metal-organic framework (MOF) synthesis assistant through embedding and searching on preselected papers. StructChem (Ouyang et al., 2024) leverages step-by-step reasoning, and iteratively refines results to solve college-level chemistry questions. Yang et al. (2023) use GPT-4 to extract experimentally measured bandgaps to train a graph neural network for accurate bandgap prediction from crystal structures. Despite the success in the specific data extraction tasks, prompt-based methods face challenges in reproducibility when the used prompts are fine-grained to work for specific edge cases. They are also still prone to hallucination and less generalizable to combine different data sources due to the deliberately designed prompt.

Several other knowledge-grounded, domain-specific language models lean on the fine-tuning approach against pre-selected data and literature. For instance, ChemGPT (Frey et al., 2022) involves fine-tuning GPT-neo on self-referencing embedded strings (SELFIES) representations of small molecules. Jablonka et al. (2024) demonstrated GPT-3 fine-tuned against online corpora could outperform purpose-trained models on classification, regression, and inverse design of high-entropy alloys and molecules. Dagdelen et al. (2024) fine-tuned GPT-3 on ~500 prompt-completion pairs to enhance LLM’s capability to extract useful information on materials chemistry from text paragraphs. However, the fine-tuned models without augmentation inherently lack awareness of the up-to-date results and any data only available after their training. Moreover, fine-tuned LLMs still suffer from limited memory retention and are prone to forget during continual training (Wang et al., 2023).

LLM function calling and tool usage An emerging class of LLM applications, including this work, take advantage of LLM text completion and instruction following capability for function calling. This approach extends LLMs with expert-curated tools to improve the quality of control for downstream applications. Coscientist (Boiko et al., 2023) combines tools such as search engines, Python, and document index for autonomous chemical research. ChemCrow (M. Bran et al., 2024) gathers multiple molecule and safety tools to enhance organic chemistry experiment and molecule design. Concurrently, Zhang et al. (2024) develop retrieval based agentic framework on their curated dataset. Ghafarollahi and Buehler (2024) propose AtomAgents for alloy design and analysis.

However, most prior works adopt *flat planning* strategy, where a single agent accesses all the available tools, resulting in a lack of self-correcting tool usage capabilities. This often leads to premature reasoning stop and summarization when the agent encounters tool usage errors. We mitigate this through *hierarchical planning* of multiple ReAct agents (see Section 4.1).

4 METHOD

4.1 HIERARCHICAL ORCHESTRATION

Overviews Flat planning, where an agent see all the available tools and related API schemas, quickly exceeds LLM context window and incurs huge cost for large-scale database like MP. To manage heterogeneous data sources and diverse types of queries, we introduce hierarchical planning, featuring a supervisor ReAct agent overseeing multiple assistant ReAct agents that have access to the tools (Figure 1). This design offers three major advantages over flat planning commonly implemented in previous works (Boiko et al., 2023; M. Bran et al., 2024): (1) modularity of the system ensures that each assistant agent can focus on domain-specific queries while the supervisor agent handles higher-level reasoning and task allocation; (2) the hierarchical structure improves

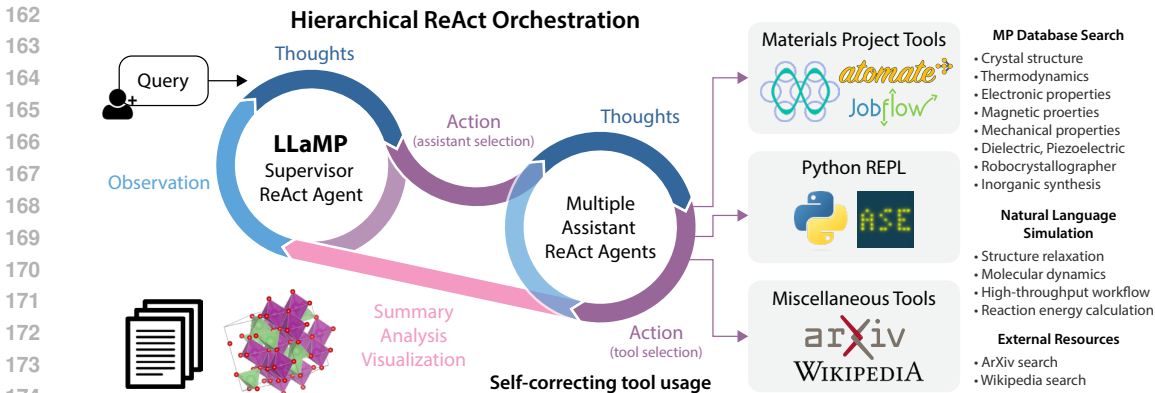


Figure 1: Hierarchical ReAct agent planning in LLaMP. Two levels of agents are deployed using a standardized LangChain interface (Chase, 2022). Supervisor ReAct agent oversees assistant ReAct agents at the bottom-level, each equipped with distinct toolkits and data/document stores to accomplish various tasks, including high-fidelity materials information retrieval, atomistic modeling and simulations, and literature search. For a detailed example, refer to Figure A.1.

the overall accuracy and efficiency by reducing the cognitive load on any individual agent; (3) by offloading specific functions to specialized agents, we minimize the context window consumption and schema parsing.

Supervisor agent The supervisor agent acts as a router and decision-maker, handling abstract logic between user requests and assistant agents. Here, we adopt ReAct on GPT-4 (Yao et al., 2023) to augment the agent’s action space \mathcal{A} with a language space \mathcal{L} to create an expanded action space of $\hat{\mathcal{A}} = \mathcal{A} \cup \mathcal{L}$. This expanded action space empowers the agent to take action $\hat{a}_t \in \mathcal{L}$ in language space that facilitate the collaboration with assistant agents to retrieve domain specific information and achieve complex downstream tasks such as molecular dynamics simulations.

Assistant agent The efficient function calling in LLMs is often hindered by the need to process complex API schemas, which can consume a significant portion of the context window. To address this, we assign a specialized ReAct agent for each specific tool or API endpoint. It reduces context window consumption, as each agent handles only the relevant schema for its task, avoiding unnecessary schema parsing. Additionally, the use of ReAct agents enables them to refine their API calls based on feedback, significantly improving task completion rates through ReAct’s iterative self-correcting mechanism.

The full list of agents and tools are defined in A.1. Each MP assistant agent employs a self-correcting ReAct mechanism, enabling agents to refine their API calls and improve task completion rates. The framework’s modularity enable a seamless integration of new assistant agents, allowing for extensibility to various materials discovery methods and experimental techniques (Luo et al., 2023; Pilia et al., 2017; Wen et al., 2023; 2024; Zeni et al., 2024).

4.2 SELF-CONSISTENCY OF RESPONSE (SCOR)

When LLMs are integrated in scientific workflows and deployed in high-stakes settings (*i.e.* self-driving labs), it is important for these models to have consistent and predictable behaviors (Liang et al., 2023). For numeric knowledge retrieval tasks, we define the following metrics:

Precision (sample standard deviation) measures the uncertainty in the model’s responses where n is the number valid responses from N trials and $\hat{\sigma}$ is the standard deviation of valid response:

$$\text{Precision} = \frac{\hat{\sigma}}{\sqrt{n}} \geq 0$$

Coefficient of Precision (CoP) maps the precision to $(0, 1]$:

$$\text{CoP} = \exp(-\text{Precision}) = \exp\left(-\frac{\hat{\sigma}}{\sqrt{n}}\right) \in (0, 1].$$

Confidence measures the ratio of generating n valid responses in N trials:

$$\text{Confidence} = \frac{n}{N}.$$

Self-consistency of Response (SCoR) is then defined as

$$\text{SCoR} = \text{CoP} \times \text{Confidence} \in [0, 1].$$

The limit of $\text{SCoR} = 1$ is reached when the model yields the same response to a given query every time. At the limit of $\text{SCoR} = 0$, the model is either very inconsistent (with large variance across the responses) or very reluctant (with low confidence) to answer the query. Despite the simplicity in definition, SCoR effectively reflects the reproducibility and practical usability of the method, which is important when the method is incorporated into broader systems where the stable and expected behaviors are prioritized. [Refer to Appendix A.2 for the detailed procedure of metric calculation.](#)

5 EXPERIMENTS

5.1 MULTIMODAL REACT AUGMENTATION

Materials design often involves multi-objective property optimization. These properties span a Pareto front where optimizing one factor incurs deterioration in others. To succeed in such tasks, combining different modalities of materials properties is necessary. LLaMP achieves this through the hierarchical orchestration of multiple ReAct agents (Yao et al., 2023). For the example question “*What’s the stiffest material with the lowest formation energy in Si-O system?*” (Figure A.1), when a query requires multimodal information and compound logic, the supervisor agent decomposes the query into multiple subtasks, delegates them to assistant agents (MPThermoExpert and MPElasticityExpert) for information retrieval, and in the final stage of reasoning integrates information from both modalities, drawing on the context in episodic memory retrieved from the assistant agents (Figure 1). This enables LLaMP to achieve various tasks step-by-step by combining multiple data sources from the Materials Project (MP) (e.g. 3D crystal structures, thermodynamic, mechanical, magnetic properties, and more listed in Appendix A.1) in a single query.

5.2 PERFORMANCE BENCHMARKS

Response quality and consistency We evaluate the performance of LLaMP, StructChem (Ouyang et al., 2024), Darwin (Xie et al., 2023), and vanilla LLMs (gpt-4, llama3-8b, gemini-1.0-pro) on material properties such as bulk modulus, formation energy, and bandgap (Figure 2, Table 1). Performance is assessed through Precision, CoP, SCoR, and MAE metrics, as defined in Section 4.2. We argue that any useful LLM agents to be included in the scientific workflow should have high SCoR and low error on the materials properties. Notably, LLaMP consistently outperforms other models, achieving the highest SCoR and the lowest errors across material properties, making it highly suitable for scientific workflows. StructChem, despite extensive prompting strategies, often fails due to a lack of necessary domain knowledge, resulting in high refusal rates when it cannot validate outputs.

For bulk modulus prediction, vanilla LLMs, particularly Llama 3-8b, frequently rely on low-fidelity online data, leading to significant deviations for elements like Cr, Mn, and Fe, compared to MP theoretical values. Interestingly, Llama 3-8b usually cites spurious reference in the responses despite largest response variance but occasionally agrees with MP values. In contrast, LLaMP outperforms vanilla LLMs and reduces the MAE from around 40 to 14.57 GPa.

Our results demonstrate that vanilla LLMs fail to provide accurate formation energy predictions, with low SCoR and high MAE ranging from 1.5 to 5.5 eV, which is impractical for material discovery requiring meV-level precision. This is not unexpected, since accurate formation energy prediction requires the computation of multiple energetics (energies of the compound itself and its elemental constituents).

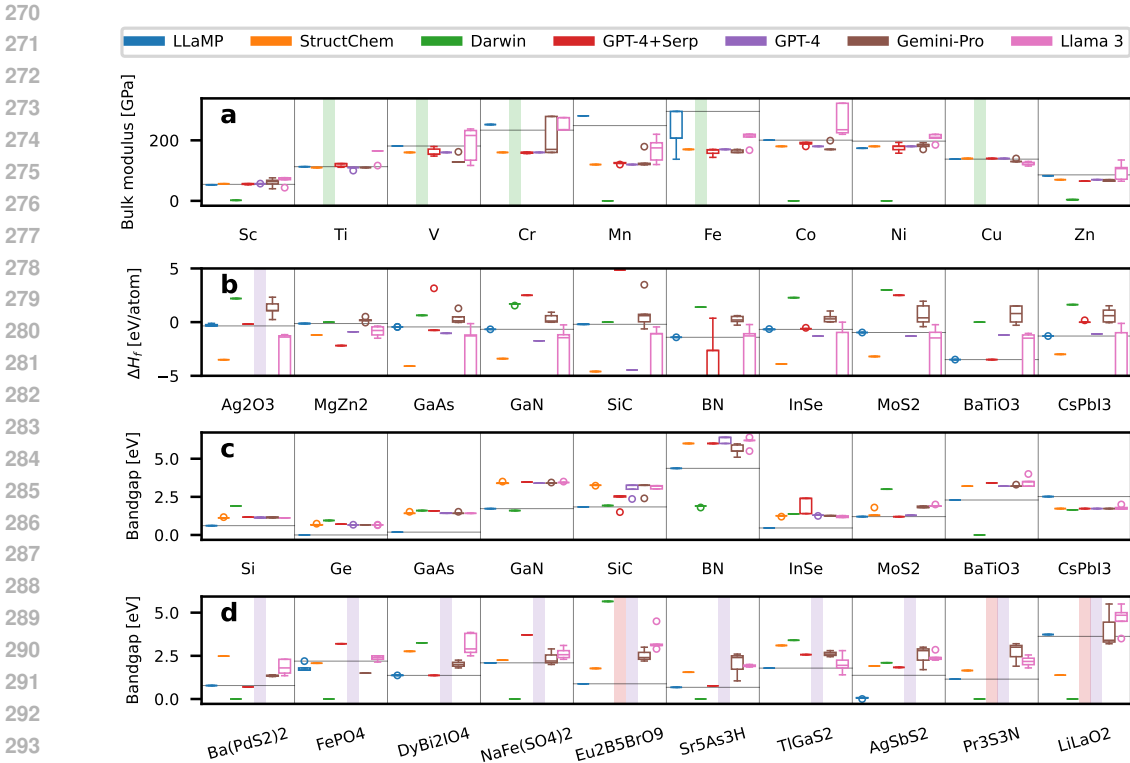


Figure 2: **Boxplot** of LLaMP RAG responses, baseline methods, and LLM intrinsic knowledge on material properties. (a) Bulk moduli, K , of 3d transition metals. (b) Formation energies, ΔH_f , of common compounds. (c) Electronic bandgaps, E_g , of common intrinsic semiconductors. (d) Electronic bandgaps of multi-element (ternary or quaternary) materials. Missing predictions are marked by shaded areas. Fliers (Outliers) are marked in circles. **Horizontal lines represent the MP reference data.** All LLaMP results use GPT-4 as backend language provider. **Method with higher SCoR has narrower distribution. LLaMP is effectively grounded on MP reference across different tasks and materials.**

In evaluating bandgaps, we query 10 common compounds and 10 multi-element materials that are less commonly encountered in the literature. Vanilla LLMs perform surprisingly well on the bandgaps of common semiconductors (Figure 2c), with expected systematic deviation from MP values retrieved by LLaMP¹. This is likely due to the extensive literature on experimental semiconductor bandgaps, which have been studied and reported for decades. On the contrary, vanilla LLMs lack intrinsic knowledge of the bandgaps for the queried multi-element materials and exhibit low confidence or refuse to make predictions (Figure 2d, Table B6.8), whereas LLaMP retrieves accurate data with a SCoR of 0.938 and correctly identifies the stable polymorph’s bandgap when multiple forms are present.

Ablation study Our framework relies on two principal components: first, factual material informatics on MP database; second, stable function calling mechanism that allows assistant agent to interact with tools. In Table 5, we examine three variants: (1) LLaMP: ReAct with MP tools; (2) GPT-4+ReAct with SerpAPI for internet browsing; (3) vanilla GPT-4. LLaMP achieved the best performance when using the complete set of MP tools, highlighting the importance of grounding in up-to-date, high-fidelity materials databases. In Section 4.1, we mentioned the importance of hierarchical planning for robust function call. Evaluating several backbone models on bulk moduli and formation energy prediction, we found LLaMP’s grounding performance correlates with the

¹Bandgaps calculated from generalized gradient approximation (GGA) functional are known to underestimate the experimental values by 40-50% (Borlido et al., 2020). Strategies to improve bandgap prediction at moderate or low computational cost will be included in MP in the future.

Table 1: Performance metrics of LLaMP and LLM baselines on the prediction of material properties. The metrics from left to right are precision (sample standard deviation), coefficient of precision (CoP), confidence, self-consistency of response (SCoR), and mean absolute error (MAE), where Materials Project are taken as the ground truth. All the tabulated values are the average metrics over five runs and the sampled materials. All LLaMP and StructChem results use GPT-4 as backend language provider. **Better method has high SCoR and MAE simultaneously.**

	Bulk Modulus K (GPa)					Formation Energy ΔH_f (eV)				
	Precision \downarrow	CoP	Confidence	SCoR \uparrow	MAE \downarrow	Precision \downarrow	CoP	Confidence	SCoR \uparrow	MAE \downarrow
LLaMP (GPT-4)	2.698	0.900	1.000	0.900	14.574	0.006	0.994	0.940	0.934	<u>0.007</u>
LLaMP (Sonnet)	1.816	0.562	1.000	0.562	15.104	0.000	1.000	1.000	1.000	0.000
LLaMP (Gemini)	5.178	0.053	1.000	0.053	16.251	0.076	0.932	0.620	0.576	0.166
LLaMP (Llama3)	12.993	0.036	0.800	0.029	50.308	0.000	1.000	0.250	0.250	1.377
StructChem	0.000	1.000	0.200	0.200	41.017	0.000	1.000	0.200	0.200	3.146
Darwin	0.001	0.999	0.500	0.499	156.266	0.003	0.997	1.000	<u>0.997</u>	2.245
GPT-4+Serp	2.221	0.833	0.300	0.433	29.937	0.025	0.977	0.560	0.791	11.669
GPT-4	0.186	0.910	1.000	<u>0.910</u>	41.225	0.000	1.000	0.180	0.200	1.680
Sonnet	0.009	0.992	1.000	0.992	41.033	0.022	0.979	1.000	0.979	294.360
Gemini-Pro	6.065	0.169	1.000	0.169	43.429	0.467	0.657	1.000	0.657	1.412
Llama 3	11.222	0.010	1.000	0.010	41.874	2.346	0.139	0.960	0.137	4.657

	Electronic Bandgap E_g - Common (eV)					Electronic Bandgap E_g - Multi-element (eV)				
	Precision \downarrow	CoP	Confidence	SCoR \uparrow	MAE \downarrow	Precision \downarrow	CoP	Confidence	SCoR \uparrow	MAE \downarrow
LLaMP (GPT-4)	0.000	1.000	0.800	0.800	0.000	0.047	0.958	0.960	0.918	0.167
LLaMP (Sonnet)	0.145	0.870	0.600	0.522	<u>0.298</u>	0.046	0.962	1.000	0.962	<u>0.304</u>
LLaMP (Gemini)	0.627	0.571	0.600	0.343	1.327	0.003	0.997	0.500	<u>0.997</u>	0.637
LLaMP (Llama3)	0.051	0.952	0.800	0.761	1.038	0.169	0.848	0.800	0.678	1.094
StructChem	0.017	0.984	1.000	0.984	0.986	0.000	1.000	0.200	0.200	0.973
Darwin	0.002	0.998	1.000	<u>0.998</u>	1.224	0.000	1.000	1.000	1.000	1.951
GPT-4+Serp	0.040	0.963	1.000	0.963	1.012	0.000	1.000	0.660	0.660	0.576
GPT-4	0.032	0.970	1.000	0.970	0.959	-	-	0.000	0.000	-
Sonnet	0.000	1.000	1.000	1.000	0.938	0.000	1.000	0.500	1.000	0.644
Gemini-Pro	0.034	0.968	1.000	0.968	0.994	0.168	0.849	0.600	0.509	0.989
Llama 3	0.042	0.960	1.000	0.960	1.053	0.182	0.836	0.860	0.719	1.091

function-calling capability of backbone LLM: Claude-3.5-Sonnet (#1) > Gemini-1.5-Flash (#24) > and Llama3-8B (#46). The number following each model refers to its ranking on the Berkeley Function-Calling Leaderboard at the time of the experiment (Yan et al., 2024).

High-fidelity and higher-order data retrieval The challenge for LLMs in excelling at knowledge- and data-intensive tasks is well-documented (Cobbe et al., 2021; Hendrycks et al., 2021; Liang et al., 2023). Figure 3 shows the prediction of LLaMP, GPT-3.5, and GPT-4 on the magnetic orderings and total magnetization of 800 materials randomly selected from all unary, binary, and ternary compounds in MP. Our result indicates that without RAG, vanilla LLMs suffer from hallucinations and misclassify the magnetic orderings of materials. LLaMP with GPT-4 as backend can counteract the intrinsic bias of GPT models, increasing the classification accuracy to 0.98 and R^2 of magnetization prediction to 0.992 (Table 2). We note that GPT-3.5 as backend, while effective for classification and other information retrieval tasks, struggles to distinguish total_magnetization from magnetization_per_formula_unit in magnetism API schema and often requests the wrong field and forgets to normalize the values. In the magnetic orderings queries, LLaMP with GPT-3.5 as backend fails to distinguish ferromagnetic (FM) and ferrimagnetic (FiM) orderings, while LLaMP with GPT-4 as backend gracefully separates the two classes (Figure 3a, d).

We further test the capability of LLaMP and LLMs for higher-order data (such as tensors, 3D crystal structures, curves). As shown in Table B6.2, GPT-3.5 hallucinates the values for the components in the elastic tensor of NaCl, with serious erroneous values such as $C_{11} = 289.2$ GPa—a significant deviation from DFT-calculated values (76 GPa). It also omits the values for $C_{22}, C_{33}, C_{55}, C_{66}$ and fails to represent the full elastic tensor in a matrix format, despite the query explicitly requesting the *full* elastic tensor. This highlights the limitation of intrinsic knowledge in LLMs to recall higher-

Table 2: Prediction performance of LLaMP, GPT-3.5, and GPT-4 on magnetic orderings and magnetization. LLaMP with GPT-4 and GPT-3.5 as backend LLM are compared.

	Magnetic Ordering		Magnetization	
	Accuracy	F1	MAE	R^2
LLaMP (GPT-4)	0.98	0.89	0.045	0.992
GPT-4	0.48	0.26	1.611	-0.201
LLaMP (GPT-3.5)	0.96	0.88	1.896	0.407
GPT-3.5	0.23	0.18	1.988	-0.024

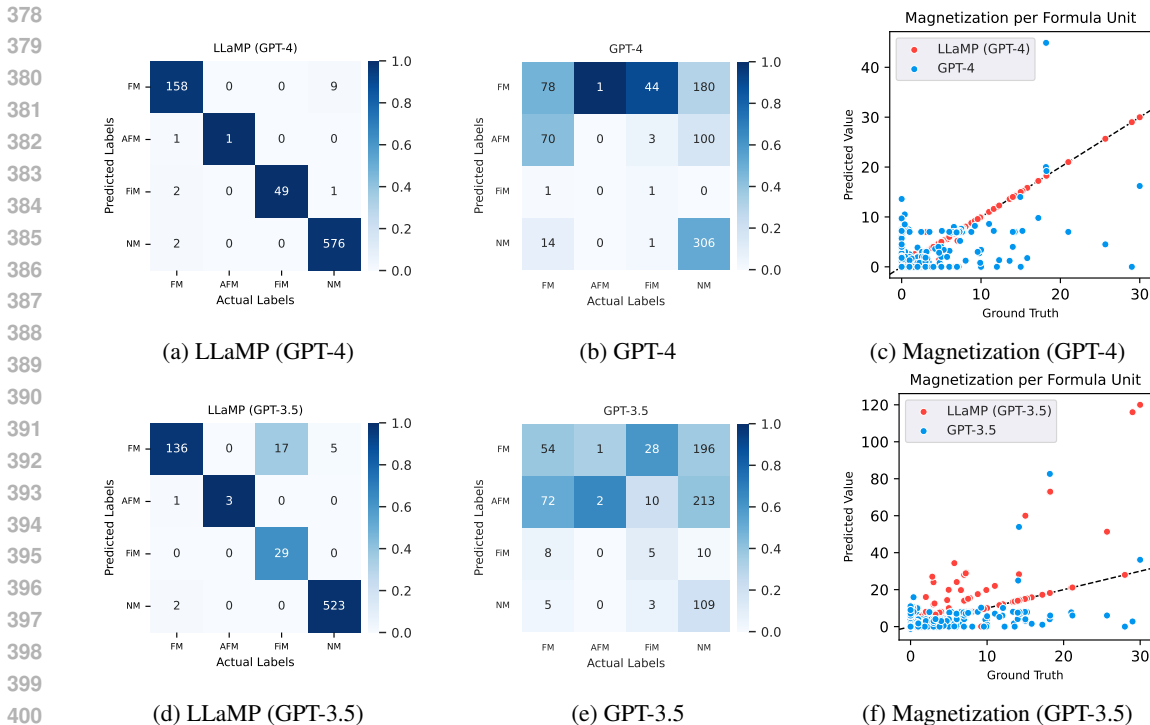


Figure 3: Prediction of LLaMP, GPT-3.5, and GPT-4 on (a,b,d,e) magnetic orderings and (c,f) total magnetization per formula unit of randomly selected materials. Confusion matrix presents the number of entries in each class. Colormap represents the percentage of correct classification.

order, more complex data for more comprehensive, holistic response.

5.3 REAL-WORLD APPLICATIONS

Inorganic synthesis recipes Empowered by the MP synthesis endpoint (Kononova et al., 2019), LLaMP can extract synthesis recipes and summarize detailed step-by-step procedures grounded on real experimental papers with associated DOI references, as demonstrated in the example queries (Table B6.9 and B6.10).

Vanilla LLMs often give seemingly correct and verbose synthesis procedures but pull irrelevant compounds into the recipes and overlook more optimal or efficient reactions. In the example of YMnO_3 (Table B6.9), GPT-3.5 suggests the possible reaction pathways from two common oxide precursors (Y_2O_3 and MnO_2). However, it pulls irrelevant lithium compounds (Li_2CO_3 and LiOH) into the recipe and overlooks the fact that metathesis reactions (Li et al., 2015; Todd et al., 2021) require less applied energy than high-temperature sintering, which relies on solid-state diffusion (Maximenko and Olevsky, 2004).

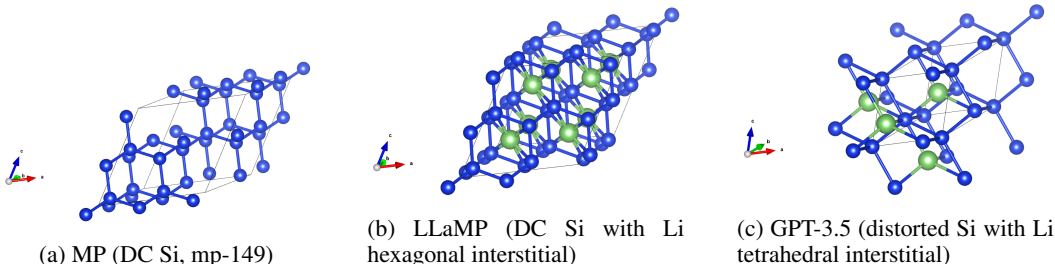
Vanilla LLMs also exhibit uncertainty about specific synthesis details, such as heating temperature, duration, cooling rate, *etc.* In some edge cases such as LiFePO_4 presented in Table B6.10, the cited

Table 3: Positive-unlabeled (PU) classification of LLaMP and baseline methods on inorganic material synthesizability. (*) Evaluations on 352,236 positive and 40,817 unlabeled compounds by Kim et al. (2024).

	Accuracy	F1	Precision	Recall
LLaMP (GPT-4)	0.800	0.773	0.895	0.680
LLaMP (Sonnet)	0.818	0.812	0.848	0.780
GPT-4	0.600	0.649	0.578	0.740
Sonnet	0.530	0.230	0.636	0.140
Llama3	0.480	0.623	0.489	0.860
Gemini	0.590	0.388	0.765	0.260
GPT-4*	-	-	0.151	0.620
GPT-3.5 (FT)*	-	-	0.558	0.951
stoi-CGNF*	-	-	0.541	0.942

432 references are associated with the real papers but the contents are dissociated from the cited titel and
 433 hallucinated from the pre-training corpus.

434
 435 We further compare the performance of LLaMP on synthesizability prediction with stoichiometric
 436 convolutional graph neural fingerprint (stoi-CGNF) (Jang et al., 2024) and fine-tuned LLMs (Kim
 437 et al., 2024). We follow the positive-unlabeled (PU) classification task proposed in (Kim et al., 2024)
 438 by randomly selecting a subset of positive (probable) and unlabeled (unlikely) inorganic compounds
 439 and compare the classification performances of LLaMP with different backend LLMs and baselines.
 440 As presented in Table 3, LLaMP effectively enhances the performances of backbone GPT-4 and
 441 Sonnet LLMs by a significant margin of 20%, with the classification precision of LLaMP (GPT-4)
 442 up to 0.895.



452
 453 Figure 4: Generation and manipulation of crystal structures using LLMs to insert an additional
 454 lithium atom at the interstitial site in diamond cubic silicon structure. Blue: Si. Green: Li. Question-
 455 answer pairs are listed in Table B6.11. Additional atoms extended through bonds are visualized.

456
 457 Table 4: Structural parameters of the generated crystals compared with diamond cubic (DC) silicon.
 458 From left to right are fractional coordinates of inserted Li atom $(x, y, z)_{\text{Li}}$, total cell volume V ,
 459 average Si-Si bond lengths l_{SiSi} , Si-Si-Si angles θ_{SiSiSi} , and Si-Li-Si angles θ_{SiLiSi} . GPT-4
 460 refuses to respond due to their safeguard against the lack of atomic structure information.

461
 462

	$(x, y, z)_{\text{Li}}$	l_{SiSi} (Å)	Error (%)	V (Å ³)	Error (%)	θ_{SiSiSi} (°)	Error (%)	θ_{SiLiSi} (°)
LLaMP	(0.5, 0.5, 0.5)	2.36	0.0	40.33	0.0	109.47	0.0	62.96
GPT-3.5	(0.5, 0.5, 0.5)	2.71	+15.0	67.05	+66.3	98.28	-10.2	67.69
GPT-4	-	-	-	-	-	-	-	-
DC Si (mp-149)		2.36		40.33		109.47		

463
 464
 465
 466
 467

468
 469 **RAG-assisted crystal generation and editing** Fine-tuned LLMs for text-encoded atomistic infor-
 470 mation have shown the capability to generate stable crystals under the constraints of atomic positions
 471 and charges (Gruver et al., 2023). In this context, we delve into the examination and comparison
 472 of the crystal generation capabilities between LLaMP and GPT-3.5, without resorting to fine-tuning
 473 or tailored prompt messages in previous work. Figure 4 showcases the structures generated by
 474 LLaMP and vanilla GPT-3.5 without RAG, both instructed to *insert one lithium atom at the tetra-*
 475 *hedral site of the diamond cubic silicon structure* (Table B6.11). Notably, both LLaMP and GPT-3.5
 476 place an additional Li atom at fractional coordinate (0.5, 0.5, 0.5). However, the Si structure re-
 477 trieved by LLaMP adheres to the MP convention, positioning two Si bases at (0.125, 0.125, 0.125)
 478 and (0.875, 0.875, 0.875). This causes the inserted Li atom to be *hexagonal interstitial* instead of
 479 *tetrahedral interstitial*.

480 GPT-3.5 locates the Li atom at the tetrahedral site given the “luckily chosen” Si bases at (0, 0, 0) and
 481 (0.25, 0.25, 0.25); however, the resulting cell volume and shape are highly distorted, and the Si-Si
 482 bond length and Si-Si-Si angle deviate significantly from the ground truth (Table 4), highlight-
 483 ing the limitations in the intrinsic encoding of LLMs for atomistic information and the challenges
 484 associated with zero-shot generation of crystal structures. In contrast, the LLaMP-retrieved MP
 485 structure serves as a robust prior, anchoring the lattice parameters of the generated structure to the
 correct values.

Language-driven simulation LLaMP equipped with Python REPL and atomistic simulation workflow package atomate2 performs well out of the box for complex multi-step simulations using pre-trained universal machine learning interatomic potential MACE-MP-0 (Batatia et al., 2023) through language instruction. As demonstrated in Appendix C.1 and Appendix C.2, LLaMP is able to follow multi-step instruction to fetch stable crystal structure from MP, generate a supercell of atomic structure, and run annealing molecular dynamics simulation with varying temperature from 300K to 800K and back to 300K. After the simulation is finished, LLaMP can read the simulation trajectories and plot the temperature profile over time (Appendix C.1).

We further test the robustness of our language-driven workflow on running MD simulations (Figure 5). A subset of 50 supercell structures were randomly created from up-to-quinary compounds in MP. Each MD simulation runs 0.1 ps with timestep of 2 fs. The timeout was set to 90 seconds. 96% workflows (SUCCESS+TIMEOUT) were successfully initiated, with 62% finished and 34% of systems exceeding 90 seconds timeout due to slow or stalled MACE-MP-0 runs (the simulation is still running without error but runs slowly). 4% simulations ran into unspecified status (UNKNOWN). We found that during these triggered workflows LLaMP asks user for approval on the precise chemical formula to fetch the structure from MP, rendering the workflow unfinished.

6 DISCUSSION

Robustness The hierarchical ReAct framework implemented here is essentially a graph of agents, or *language graph*, with one central node (supervisor) in connection with many satellite nodes (assistants). The implementation of ReAct for the assistant agents enables self-correcting tool usages and fortifies the robustness of data retrieval. As presented in Figure A.1c, MPThermoExpert initially misunderstood the schema at the first trial and filled in the formula field with Si-O, an invalid input but a valid one for chemical system (chemsys) field. The observation step (step 4) allows MPThermoExpert to handle exceptions and to refine the correct input fields after adaptation (step 6). Storing (Retrieving) question-answer and query-argument pairs to (from) vector databases could further reduce the number of trial-and-error steps, and the stored pairs can be used to refine foundation LLMs to improve function calling quality.

Limitation We recognize the effectiveness of LLaMP’s framework relies on backbone LLM’s function calling and reasoning capabilities. Sometimes LLMs misunderstand the description of schemas and therefore yield unexpected behaviors. For example, `sort_fields` argument allows sorting the returned documents in ascending order or descending order if the field is prefixed with -, but LLMs sometimes mistake the sign and sort in the opposite order. Other example failure or safeguard modes are presented in Appendix A.3. The correctness of LLaMP is also subject to the quality of theoretical prediction and the comprehensiveness of the data in MP. Other than the underpredicted bandgaps by GGA functional, MP’s ongoing effort to search all possible magnetic configurations is also not complete. Most of the existing calculations in MP start from high-spin ferromagnetic configurations, which may overlook many antiferromagnetic ground states below the current energy convex hull. While MP is one of the most comprehensive materials databases, the available crystal structures on MP are not exhaustive but continuously expanding (Merchant et al., 2023), and would be benefited from additional intermetallic compounds and high-entropy materials from other databases such as AFLOW, OQMD, NOMAD, etc. (Curtarolo et al., 2012; Kirklin et al., 2015; Scheidgen et al., 2023). Furthermore, Kohn-Sham DFT theory is insufficient in some cases, and a higher level of theory is needed. Currently LLaMP only supports a few atomate2 workflows with machine learning force fields and VASP calculations. More diverse electronic calculation methods and workflows will be supported in the future work.

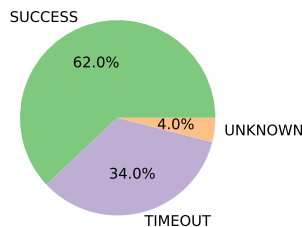


Figure 5: The final four statuses (SUCCESS, TIMEOUT, FAILURE, UNKNOWN) of trial language-driven MD simulation runs on random MP supercell structures. LLaMP successfully initiated 96% (SUCCESS+TIMEOUT) of all the simulations within 90 second timeout window.

Summary We present a hierarchical agentic framework, LLaMP, based on ReAct to extract and manipulate material informatics through few-shot generalization. By grounding thoughts and actions with high-fidelity information, LLaMP showcases the ability to integrate various modalities of material properties and perform logical inferences to accomplish assigned tasks, all without the need for fine-tuning. In essence, the proposed LangChain framework holds the potential to expand its applicability to multiple data sources, encompassing both theoretical computations and experimental data, **knowledge graph databases** (Venugopal and Olivetti, 2024; Ye et al., 2024), and real-world laboratories by incorporating additional assistant agents for data retrieval and robot control (Fei et al., 2024). LLaMP functions as a knowledge-aware agent, empowering users to navigate and manipulate complex materials informatics. In the context of self-driving labs (Boiko et al., 2023; Szymanski et al., 2023), LLM agents with multimodal data sources, sensors, and actors may improve their decision making and operation (Miret and Krishnan, 2024). As new tools continue to emerge, there is an exciting avenue for further exploration to ascertain if this framework can effectively facilitate scientific hypothesis generation and guide data-driven experiments.

REFERENCES

- Y. Bang et al. A Multitask, Multilingual, Multimodal Evaluation of ChatGPT on Reasoning, Hallucination, and Interactivity, Nov. 2023. URL <http://arxiv.org/abs/2302.04023>. arXiv:2302.04023 [cs].
- I. Batatia et al. A foundation model for atomistic materials chemistry, Dec. 2023. URL <http://arxiv.org/abs/2401.00096>. arXiv:2401.00096 [cond-mat, physics:physics].
- D. A. Boiko, R. MacKnight, B. Kline, and G. Gomes. Autonomous chemical research with large language models. *Nature*, 624(7992):570–578, Dec. 2023. ISSN 1476-4687. doi: 10.1038/s41586-023-06792-0. URL <https://www.nature.com/articles/s41586-023-06792-0>. Number: 7992 Publisher: Nature Publishing Group.
- P. Borlido et al. Exchange-correlation functionals for band gaps of solids: benchmark, reparametrization and machine learning. *npj Computational Materials*, 6(1):1–17, July 2020. ISSN 2057-3960. doi: 10.1038/s41524-020-00360-0. URL <https://www.nature.com/articles/s41524-020-00360-0>. Number: 1 Publisher: Nature Publishing Group.
- H. Chase. LangChain, Oct. 2022. URL <https://github.com/langchain-ai/langchain>.
- K. Cobbe et al. Training Verifiers to Solve Math Word Problems, Nov. 2021. URL <http://arxiv.org/abs/2110.14168>. arXiv:2110.14168 [cs].
- S. Curtarolo et al. AFLOW: An automatic framework for high-throughput materials discovery. *Computational Materials Science*, 58:218–226, June 2012. ISSN 0927-0256. doi: 10.1016/j.commatsci.2012.02.005. URL <https://www.sciencedirect.com/science/article/pii/S0927025612000717>.
- J. Dagdelen et al. Structured information extraction from scientific text with large language models. *Nature Communications*, 15(1):1418, Feb. 2024. ISSN 2041-1723. doi: 10.1038/s41467-024-45563-x. URL <https://www.nature.com/articles/s41467-024-45563-x>. Publisher: Nature Publishing Group.
- Y. Fei et al. AlabOS: a Python-based reconfigurable workflow management framework for autonomous laboratories. *Digital Discovery*, 3(11):2275–2288, 2024. ISSN 2635-098X. doi: 10.1039/D4DD00129J. URL <https://xlink.rsc.org/?DOI=D4DD00129J>.
- N. Frey et al. Neural Scaling of Deep Chemical Models, May 2022. URL <https://chemrxiv.org/engage/chemrxiv/article-details/627bddd544bdd532395fb4b5>.
- A. M. Ganose and A. Jain. Robocrystallographer: automated crystal structure text descriptions and analysis. *MRS Communications*, 9(3):874–881, Sept. 2019. ISSN 2159-6867. doi: 10.1557/mrc.2019.94. URL <https://doi.org/10.1557/mrc.2019.94>.
- A. Ghafarollahi and M. J. Buehler. AtomAgents: Alloy design and discovery through physics-aware multi-modal multi-agent artificial intelligence, July 2024. URL <http://arxiv.org/abs/2407.10022>. arXiv:2407.10022.

- 594 N. Gruver et al. Fine-Tuned Language Models Generate Stable Inorganic Materials as Text. Nov.
595 2023. URL <https://openreview.net/forum?id=0r5DE2ZSwJ>.
- 596
- 597 T. Gupta, M. Zaki, N. M. A. Krishnan, and Mausam. MatSciBERT: A materials domain language
598 model for text mining and information extraction. *npj Computational Materials*, 8(1):1–11, May
599 2022. ISSN 2057-3960. doi: 10.1038/s41524-022-00784-w. URL [https://www.nature.com/
600 articles/s41524-022-00784-w](https://www.nature.com/articles/s41524-022-00784-w). Number: 1 Publisher: Nature Publishing Group.
- 601 D. Hendrycks et al. Measuring Massive Multitask Language Understanding, Jan. 2021. URL [http:
602 //arxiv.org/abs/2009.03300](http://arxiv.org/abs/2009.03300). arXiv:2009.03300 [cs].
- 603
- 604 K. Hira et al. Reconstructing the materials tetrahedron: challenges in materials information extrac-
605 tion. *Digital Discovery*, 3(5):1021–1037, 2024. ISSN 2635-098X. doi: 10.1039/D4DD00032C.
606 URL <https://xlink.rsc.org/?DOI=D4DD00032C>.
- 607 K. M. Jablonka, P. Schwaller, A. Ortega-Guerrero, and B. Smit. Leveraging large language mod-
608 els for predictive chemistry. *Nature Machine Intelligence*, 6(2):161–169, Feb. 2024. ISSN
609 2522-5839. doi: 10.1038/s42256-023-00788-1. URL [https://www.nature.com/articles/
610 s42256-023-00788-1](https://www.nature.com/articles/s42256-023-00788-1). Publisher: Nature Publishing Group.
- 611 A. Jain et al. Commentary: The Materials Project: A materials genome approach to accelerating
612 materials innovation. *APL Materials*, 1(1):011002, July 2013. ISSN 2166-532X. doi: 10.1063/1.
613 4812323. URL <https://doi.org/10.1063/1.4812323>.
- 614
- 615 J. Jang et al. Synthesizability of materials stoichiometry using semi-supervised learning. *Matter*, 7
616 (6):2294–2312, June 2024. ISSN 2590-2393, 2590-2385. doi: 10.1016/j.matt.2024.05.002. URL
617 [https://www.cell.com/matter/abstract/S2590-2385\(24\)00227-3](https://www.cell.com/matter/abstract/S2590-2385(24)00227-3). Publisher: Elsevier.
- 618 S. Kim, Y. Jung, and J. Schrier. Large Language Models for Inorganic Synthesis Predictions. *Journal
619 of the American Chemical Society*, 146(29):19654–19659, July 2024. ISSN 0002-7863. doi:
620 10.1021/jacs.4c05840. URL <https://doi.org/10.1021/jacs.4c05840>. Publisher: American
621 Chemical Society.
- 622 S. Kirklin et al. The Open Quantum Materials Database (OQMD): assessing the accuracy of
623 DFT formation energies. *npj Computational Materials*, 1(1):1–15, Dec. 2015. ISSN 2057-
624 3960. doi: 10.1038/npjcompumats.2015.10. URL [https://www.nature.com/articles/
625 npjcompumats201510](https://www.nature.com/articles/npjcompumats201510). Publisher: Nature Publishing Group.
- 626
- 627 O. Kononova et al. Text-mined dataset of inorganic materials synthesis recipes. *Scientific Data*, 6
628 (1):203, Oct. 2019. ISSN 2052-4463. doi: 10.1038/s41597-019-0224-1. URL [https://www.
629 nature.com/articles/s41597-019-0224-1](https://www.nature.com/articles/s41597-019-0224-1). Number: 1 Publisher: Nature Publishing Group.
- 630 G. Kresse and J. Furthmüller. Efficient iterative schemes for ab initio total-energy calculations
631 using a plane-wave basis set. *Physical Review B*, 54(16):11169–11186, Oct. 1996. doi: 10.
632 1103/PhysRevB.54.11169. URL <https://link.aps.org/doi/10.1103/PhysRevB.54.11169>.
633 Publisher: American Physical Society.
- 634 P. Lewis et al. Retrieval-Augmented Generation for Knowledge-Intensive NLP Tasks. In
635 *Advances in Neural Information Processing Systems*, volume 33, pages 9459–9474. Cur-
636 ran Associates, Inc., 2020. URL [https://proceedings.neurips.cc/paper/2020/hash/
637 6b493230205f780e1bc26945df7481e5-Abstract.html](https://proceedings.neurips.cc/paper/2020/hash/6b493230205f780e1bc26945df7481e5-Abstract.html).
- 638
- 639 P. Lewis et al. Retrieval-Augmented Generation for Knowledge-Intensive NLP Tasks, Apr. 2021.
640 URL <http://arxiv.org/abs/2005.11401>. arXiv:2005.11401 [cs] version: 4.
- 641 J. Li et al. True Composition and Structure of Hexagonal “YAIO3”, Actually Y3Al3O8CO3. *Inor-
642 ganic Chemistry*, 54(3):837–844, Feb. 2015. ISSN 0020-1669. doi: 10.1021/ic502027k. URL
643 <https://doi.org/10.1021/ic502027k>. Publisher: American Chemical Society.
- 644
- 645 P. Liang et al. Holistic Evaluation of Language Models, Oct. 2023. URL [http://arxiv.org/abs/
646 2211.09110](http://arxiv.org/abs/2211.09110). arXiv:2211.09110 [cs].
- 647 Y. Luo, C. Liu, and S. Ji. Towards Symmetry-Aware Generation of Periodic Materials, July 2023.
URL <https://arxiv.org/abs/2307.02707v2>.

- 648 A. M. Bran et al. Augmenting large language models with chemistry tools. *Nature Machine*
649 *Intelligence*, pages 1–11, May 2024. ISSN 2522-5839. doi: 10.1038/s42256-024-00832-8.
650 URL <https://www.nature.com/articles/s42256-024-00832-8>. Publisher: Nature Publish-
651 ing Group.
- 652 A. Mallen et al. When Not to Trust Language Models: Investigating Effectiveness of Para-
653 metric and Non-Parametric Memories, July 2023. URL <http://arxiv.org/abs/2212.10511>.
654 arXiv:2212.10511 [cs].
- 655 A. L. Maximenko and E. A. Olevsky. Effective diffusion coefficients in solid-state sintering. *Acta*
656 *Materialia*, 52(10):2953–2963, June 2004. ISSN 1359-6454. doi: 10.1016/j.actamat.2004.02.
657 042. URL <https://www.sciencedirect.com/science/article/pii/S1359645404001326>.
- 658 A. Merchant et al. Scaling deep learning for materials discovery. *Nature*, pages 1–6, Nov.
659 2023. ISSN 1476-4687. doi: 10.1038/s41586-023-06735-9. URL [https://www.nature.com/](https://www.nature.com/articles/s41586-023-06735-9)
660 [articles/s41586-023-06735-9](https://www.nature.com/articles/s41586-023-06735-9). Publisher: Nature Publishing Group.
- 661 S. Miret and N. M. A. Krishnan. Are LLMs Ready for Real-World Materials Discovery?, Sept.
662 2024. URL <http://arxiv.org/abs/2402.05200>. arXiv:2402.05200 [cond-mat].
- 663 S. Ouyang et al. Structured Chemistry Reasoning with Large Language Models, Feb. 2024. URL
664 <http://arxiv.org/abs/2311.09656>. arXiv:2311.09656 [cs].
- 665 G. Pilania, J. E. Gubernatis, and T. Lookman. Multi-fidelity machine learning models for accurate
666 bandgap predictions of solids. *Computational Materials Science*, 129:156–163, Mar. 2017. ISSN
667 0927-0256. doi: 10.1016/j.commatsci.2016.12.004. URL [https://www.sciencedirect.com/](https://www.sciencedirect.com/science/article/pii/S0927025616306188)
668 [science/article/pii/S0927025616306188](https://www.sciencedirect.com/science/article/pii/S0927025616306188).
- 669 M. P. Polak and D. Morgan. Extracting Accurate Materials Data from Research Papers with Conversa-
670 tional Language Models and Prompt Engineering, June 2023. URL [http://arxiv.org/abs/](http://arxiv.org/abs/2303.05352)
671 [2303.05352](http://arxiv.org/abs/2303.05352). arXiv:2303.05352 [cond-mat].
- 672 A. Radford et al. Learning Transferable Visual Models From Natural Language Supervision, Feb.
673 2021. URL <http://arxiv.org/abs/2103.00020>. arXiv:2103.00020 [cs].
- 674 M. Scheidgen et al. NOMAD: A distributed web-based platform for managing materials science
675 research data. *Journal of Open Source Software*, 8(90):5388, Oct. 2023. ISSN 2475-9066. doi:
676 10.21105/joss.05388. URL <https://joss.theoj.org/papers/10.21105/joss.05388>.
- 677 M. Schilling-Wilhelmi et al. From Text to Insight: Large Language Models for Materials Science
678 Data Extraction, July 2024. URL <http://arxiv.org/abs/2407.16867>. arXiv:2407.16867.
- 679 Y. Shao et al. Advances in molecular quantum chemistry contained in the Q-Chem 4 pro-
680 gram package. *Molecular Physics*, 113(2):184–215, Jan. 2015. ISSN 0026-8976. doi:
681 10.1080/00268976.2014.952696. URL [https://www.tandfonline.com/doi/full/10.1080/](https://www.tandfonline.com/doi/full/10.1080/00268976.2014.952696)
682 [00268976.2014.952696](https://www.tandfonline.com/doi/full/10.1080/00268976.2014.952696). Publisher: Taylor & Francis.
- 683 Y. Song, S. Miret, and B. Liu. MatSci-NLP: Evaluating Scientific Language Models on Materials
684 Science Language Tasks Using Text-to-Schema Modeling, May 2023. URL [http://arxiv.org/](http://arxiv.org/abs/2305.08264)
685 [abs/2305.08264](http://arxiv.org/abs/2305.08264). arXiv:2305.08264.
- 686 E. W. C. Spotte-Smith et al. A database of molecular properties integrated in the Materi-
687 als Project, Oct. 2023. URL [https://chemrxiv.org/engage/chemrxiv/article-details/](https://chemrxiv.org/engage/chemrxiv/article-details/651a3302ade1178b247ee6d1)
688 [651a3302ade1178b247ee6d1](https://chemrxiv.org/engage/chemrxiv/article-details/651a3302ade1178b247ee6d1).
- 689 N. J. Szymanski et al. An autonomous laboratory for the accelerated synthesis of novel materials.
690 *Nature*, 624(7990):86–91, Dec. 2023. ISSN 1476-4687. doi: 10.1038/s41586-023-06734-w.
691 URL <https://www.nature.com/articles/s41586-023-06734-w>. Number: 7990 Publisher:
692 Nature Publishing Group.
- 693 P. K. Todd et al. Selectivity in Yttrium Manganese Oxide Synthesis via Local Chemical Potentials
694 in Hyperdimensional Phase Space. *Journal of the American Chemical Society*, 143(37):15185–
695 15194, Sept. 2021. ISSN 0002-7863. doi: 10.1021/jacs.1c06229. URL [https://doi.org/10.](https://doi.org/10.1021/jacs.1c06229)
696 [1021/jacs.1c06229](https://doi.org/10.1021/jacs.1c06229). Publisher: American Chemical Society.

- 702 V. Tshitoyan et al. Unsupervised word embeddings capture latent knowledge from materials
703 science literature. *Nature*, 571(7763):95–98, July 2019. ISSN 1476-4687. doi: 10.1038/
704 s41586-019-1335-8. URL <https://www.nature.com/articles/s41586-019-1335-8>. Num-
705 ber: 7763 Publisher: Nature Publishing Group.
- 706 V. Venugopal and E. Olivetti. MatKG: An autonomously generated knowledge graph in Material Sci-
707 ence. *Scientific Data*, 11(1):217, Feb. 2024. ISSN 2052-4463. doi: 10.1038/s41597-024-03039-z.
708 URL <https://www.nature.com/articles/s41597-024-03039-z>. Publisher: Nature Publish-
709 ing Group.
- 710 W. Wang et al. Augmenting Language Models with Long-Term Memory, June 2023. URL <http://arxiv.org/abs/2306.07174>. arXiv:2306.07174 [cs].
- 711 M. Wen et al. Chemical reaction networks and opportunities for machine learning. *Nature Com-
712 putational Science*, 3(1):12–24, Jan. 2023. ISSN 2662-8457. doi: 10.1038/s43588-022-00369-z.
713 URL <https://www.nature.com/articles/s43588-022-00369-z>. Publisher: Nature Publish-
714 ing Group.
- 715 M. Wen et al. An equivariant graph neural network for the elasticity tensors of all seven crys-
716 tal systems. *Digital Discovery*, 3(5):869–882, May 2024. ISSN 2635-098X. doi: 10.
717 1039/D3DD00233K. URL [https://pubs.rsc.org/en/content/articlelanding/2024/dd/
718 d3dd00233k](https://pubs.rsc.org/en/content/articlelanding/2024/dd/d3dd00233k). Publisher: RSC.
- 719 T. Xie et al. DARWIN Series: Domain Specific Large Language Models for Natural Sci-
720 ence, Aug. 2023. URL <http://arxiv.org/abs/2308.13565>. arXiv:2308.13565 [cond-mat,
721 physics:physics].
- 722 Z. Xu, S. Jain, and M. Kankanhalli. Hallucination is Inevitable: An Innate Limitation of Large
723 Language Models, Jan. 2024. URL <http://arxiv.org/abs/2401.11817>. arXiv:2401.11817
724 [cs].
- 725 F. Yan et al. Berkeley Function Calling Leaderboard. 2024. URL [https://gorilla.cs.berkeley.
726 edu/blogs/8.berkeley_function_calling_leaderboard.html](https://gorilla.cs.berkeley.edu/blogs/8.berkeley_function_calling_leaderboard.html).
- 727 S. Yang et al. Accurate Prediction of Experimental Band Gaps from Large Language Model-Based
728 Data Extraction. Nov. 2023. URL <https://openreview.net/forum?id=oRKWhmtUG6>.
- 729 S. Yao et al. ReAct: Synergizing Reasoning and Acting in Language Models, Mar. 2023. URL
730 <http://arxiv.org/abs/2210.03629>. arXiv:2210.03629 [cs].
- 731 Y. Ye et al. Construction and Application of Materials Knowledge Graph in Multidisciplinary Ma-
732 terials Science via Large Language Model, Sept. 2024. URL [http://arxiv.org/abs/2404.
733 03080](http://arxiv.org/abs/2404.03080). arXiv:2404.03080.
- 734 D. Zagorac et al. Recent developments in the Inorganic Crystal Structure Database: theoretical
735 crystal structure data and related features. *Journal of Applied Crystallography*, 52(5):918–925,
736 Oct. 2019. ISSN 1600-5767. doi: 10.1107/S160057671900997X. URL [https://journals.
737 iucr.org/j/issues/2019/05/00/in5024/](https://journals.iucr.org/j/issues/2019/05/00/in5024/). Publisher: International Union of Crystallography.
- 738 M. Zaki, Jayadeva, Mausam, and N. M. A. Krishnan. MaScQA: A Question Answering Dataset
739 for Investigating Materials Science Knowledge of Large Language Models, Aug. 2023. URL
740 <http://arxiv.org/abs/2308.09115>. arXiv:2308.09115.
- 741 C. Zeni et al. MatterGen: a generative model for inorganic materials design, Jan. 2024. URL
742 <http://arxiv.org/abs/2312.03687>. arXiv:2312.03687 [cond-mat].
- 743 H. Zhang et al. HoneyComb: A Flexible LLM-Based Agent System for Materials Science, Aug.
744 2024. URL <http://arxiv.org/abs/2409.00135>. arXiv:2409.00135.
- 745 Z. Zheng et al. ChatGPT Chemistry Assistant for Text Mining and Prediction of MOF Syn-
746 thesis. *Journal of the American Chemical Society*, 145(32):18048–18062, Aug. 2023. ISSN
747 0002-7863, 1520-5126. doi: 10.1021/jacs.3c05819. URL <http://arxiv.org/abs/2306.11296>.
748 arXiv:2306.11296 [cond-mat, physics:physics].

A SUPPLEMENTARY INFORMATION

A.1 LIST OF IMPLEMENTED ASSISTANT AGENTS AND TOOLS

Here we provide the comprehensive list of implemented **assistant agents** and tools. Note that **MP Assistants** are highly modular so it is very trivial to support extra API endpoints from <https://api.materialsproject.org/docs>.

- **MPSummaryExpert**: summary provides amalgamated data for a material by combining subsets of data from many of the other API endpoints.
- **MPThermoExpert**: thermo provides computed thermodynamic data for a material such as formation energy and energy above hull.
- **MPElasticityExpert**: elasticity provides bulk, shear, and Young’s modulus, poisson ratio, and universal anisotropy index.
- **MPMagnetismExpert**: magnetism provides computed magnetic ordering related data.
- **MPDielectricExpert**: dielectric provides computed dielectric data from density functional perturbation theory.
- **MPPiezoelectricExpert**: piezoelectric provides computed piezoelectric data from density functional perturbation theory.
- **MPElectronicExpert**: electronic_structure provides computed electronic structure related data for a material such as band gap and fermi level. Python objects for line-mode band structures, density of states, and fermi surfaces are also available.
- **MPSynthesisExpert**: synthesis provides a synthesis recipes for materials extracted from literature using text mining and natural language processing techniques.
- **MPStructureRetriever**: MaterialsStructureText fetches and saves pymatgen Structure objects to local JSON files.
- **MLFFAgent**: MLFFMD runs molecular dynamics simulations using pre-trained machine learning force fields; MLFFElastic calculates the elastic constants of a given material using pre-trained machine learning force fields.
- PythonREPLTool: Python REPL that LLMs could run the generated script.
- ArxivQueryRun: LangChain built-in tool that LLMs can use to send API request to ArXiv.
- WikipediaQueryRun: LangChain built-in tool that LLMs can use to send API request to Wikipedia.

A.2 METRIC CALCULATION IN TABLE 1 AND FIGURE 2

The following procedures are adopted to calculate the metrics for material property regression benchmarks presented in Table 1 and Figure 2:

1. Each method was presented with the same query asking for the property of multiple materials. Here we ask each method for bulk modulus, formation energy, and electronic bandgap of ten materials. For example, “What are the bulk moduli of the following metals: Sc, Ti, V, Cr, Mn, Fe, Co, Ni, Cu, Zn?”.
2. Repeat the same query for five times and collect the responses.
3. The numerical values are extracted and formatted into 2D arrays with the aid by LLMs. If the range is provided in the response (*e.g.* Llama 3), the median value was used.

4. Calculate Precision, CoP, Confidence, and SCoR for each method across five trials on all materials. The code is provided and the pseudocode can be written as follows:

Input: arr (2D array of five responses for different materials)
 $n \leftarrow$ count of valid responses (non-NaN values) in each column of arr
 $prec \leftarrow \frac{\text{nanstd}(\text{arr}, \text{axis}=0)}{\sqrt{n}}$
 $cop \leftarrow \text{mean}(\exp(-prec))$
 $conf \leftarrow \text{mean}\left(\frac{n}{\# \text{ of trials } N}\right)$
 $scor \leftarrow \begin{cases} 0 & \text{if } conf = 0 \text{ for all columns} \\ cop \times conf & \text{otherwise} \end{cases}$
 $prec \leftarrow \text{mean}(prec)$
Output: prec, cop, conf, scor

A.3 SAFEGUARD OR FAILURE MODES

- Question: What is the bulk modulus of stainless steel?** ambiguous chemical formula

LLaMP: Stainless steel is an alloy with a composition that can vary widely, including elements like iron, chromium, nickel, and molybdenum. Because of this variability, it does not have a single chemical formula or a unique Materials Project ID, and its bulk modulus can significantly vary based on its exact composition and heat treatment. The Materials Project database, focusing on inorganic crystalline materials, may not provide specific data on complex alloys like stainless steel. For precise values of the bulk modulus, consulting specific datasheets or literature on the type of stainless steel in question is recommended.
- Question: How to synthesize Y2Be2Fe(SiO5)2** data unavailable

LLaMP: Currently, there are no synthesis recipes available in the Materials Project database for Y2Be2Fe(SiO5)2.
- Question: What’s the phonon bandgap of Ac2HgGe** computed property unavailable

LLaMP: The material Ac2HgGe, with a Materials Project ID of mp-861872, does not have its phonon bandgap information directly available through the Materials Project database. For detailed phonon properties, further analysis using specialized phonon calculation tools or databases would be necessary.

Table 5: Performance of LLaMP with different backbone LLMs and ablation of ReAct agent with MP API and SerpAPI tools.

	Bulk Moduli K (GPa)					Formation Energies ΔH_f (eV)				
	Precision↓	CoP	Confidence	SCoR↑	MAE↓	Precision↓	CoP	Confidence	SCoR↑	MAE↓
LLaMP	2.698	0.900	1.000	0.900	14.574	0.007	0.993	0.960	<u>0.953</u>	0.009
LLaMP (Sonnet)	1.345	0.702	0.867	<u>0.608</u>	<u>16.121</u>	0.000	1.000	1.000	1.000	0.000
LLaMP (Gemini-1.5)	21.586	0.217	1.000	0.217	64.324	0.390	0.718	0.560	0.402	0.531
LLaMP (Llama 3)	7.314	0.327	0.800	0.261	47.386	0.413	0.721	1.000	0.721	3.062
GPT-4+Serp	2.222	0.352	1.000	0.352	41.742	5.947	0.745	1.000	0.745	8.214
GPT-4	0.186	0.910	1.000	0.910	41.225	0.000	1.000	0.180	0.180	1.680

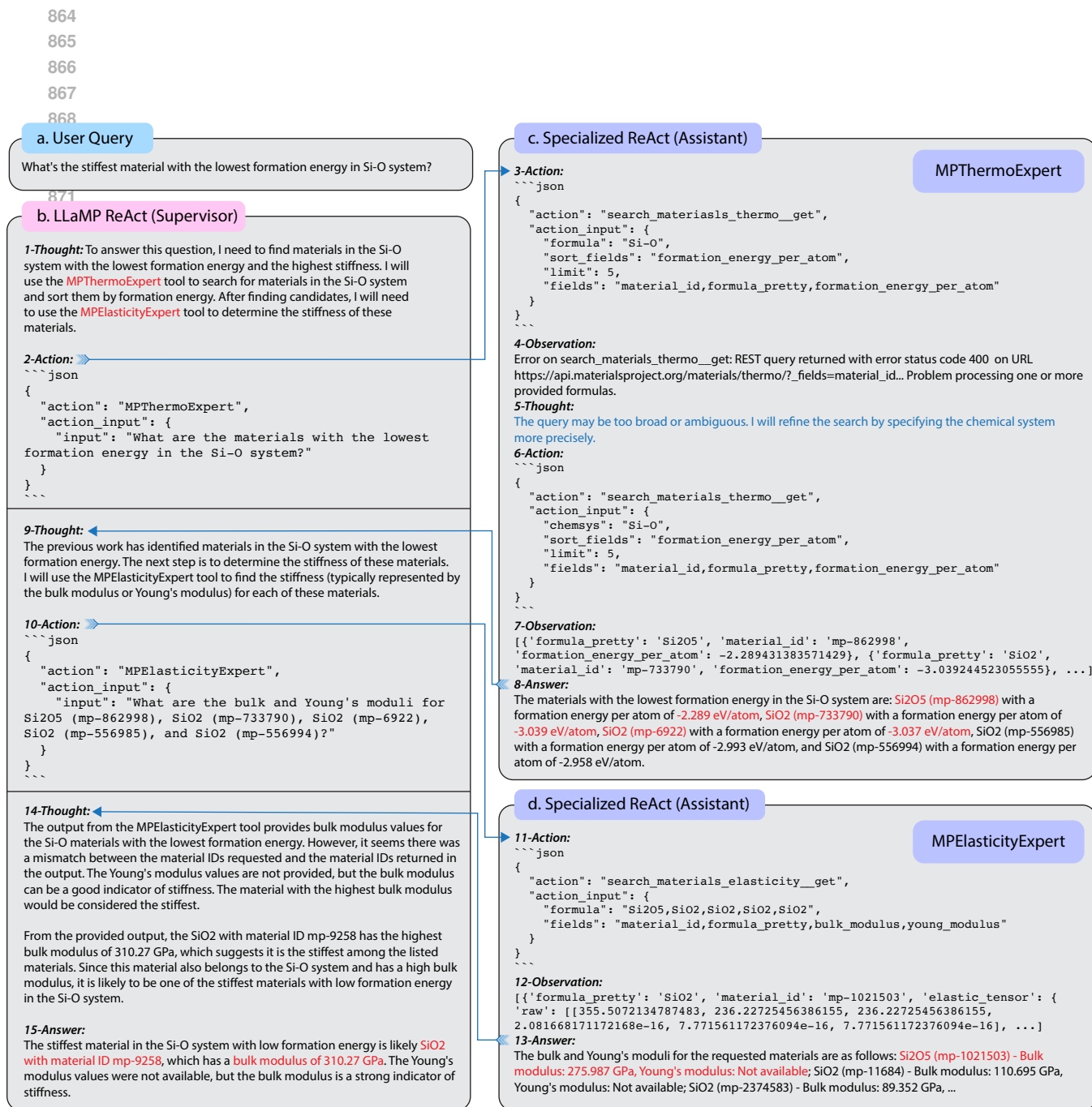


Figure A.1: Multimodal retrieval-augmented generation for materials informatics. (a) User query. (b) Supervisor ReAct agent capable of handling multiple assistant agents and high-level reasoning. (c-d) Assistant ReAct agents executing function calling and summarization. (c) **MPThermoExpert** and (d) **MPElasticityExpert** have access to the API schemas of thermo and elasticity endpoints on Materials Project, respectively. The selected details are highlighted in red, demonstrating the capabilities of RAG and ReAct implemented in LLaMP. The blue texts show LLaMP assistant ReAct agent can handle API calling errors and self-correct the input query accordingly.

918 A.4 PROMPT TEMPLATE

919 We use the ReAct template `hwchase17/react-multi-input-json` from LangChain Hub
 920 (<https://smith.langchain.com/hub/hwchase17/react-json>) as follows:

```

921 Answer the following questions as best you can. You have access to the following
922 tools:
923
924 {tools}
925
926 The way you use the tools is by specifying a JSON blob.
927 Specifically, this JSON should have an 'action' key (with the name of the tool to
928 use) and an 'action_input' key (with the input to the tool going here).
929
930 The only values that should be in the "action" field are: {tool_names}
931
932 The $JSON_BLOB should only contain a SINGLE action, do NOT return a list of multiple
933 actions. Here is an example of a valid $JSON_BLOB:
934
935 ```
936 {{
937   "action": $TOOL_NAME,
938   "action_input": $INPUT
939 }}
940 ```
941
942 ALWAYS use the following format:
943
944 Question: the input question you must answer
945 Thought: you should always think about what to do
946 Action:
947 ```
948 $JSON_BLOB
949 ```
950 Observation: the result of the action
951 ... (this Thought/Action/Observation can repeat N times)
952 Thought: I now know the final answer
953 Final Answer: the final answer to the original input question
954
955 Begin! Reminder to always use the exact characters 'Final Answer' when responding.
  
```

956 The above system prompt message is prepended with the following solicitation to guide the super-
 957 visor agent:

```

958 You name is LLaMP and you are a helpful agent that can consult materials-related
959 data through Materials Project (MP) database, arXiv, Wikipedia, and run
960 calculations/simulations via a python REPL and MP atomate2 computational
961 workflow.
962
963 If you get an error, debug your code and try again. Only use the output of your code
964 to answer the question. Ask user to clarify their queries if needed. Please
965 note that you don't have direct control over MP but through multiple assistant
966 agents to help you. You need to provide complete context in the input for
967 assistants to do their job. REFINE and CRITQUE the output of the assistants if
968 needed. You can end the conversation by saying "Bye".
  
```

972
973
974
975
976
977
978
979
980
981
982
983
984
985
986
987
988
989
990
991
992
993
994
995
996
997
998
999
1000
1001
1002
1003
1004

B SAMPLE QUESTIONS

Table 6: QA comparison between LLaMP and GPT-3.5.

	Question	Answer	
		LLaMP	GPT-3.5
B6.1	What are the bulk moduli of the following metals: Sc, Ti, V, Cr, Mn, Fe, Co, Ni, Cu, Zn?	<p>The bulk moduli of the metals you asked for are as follows (in GPa): - Scandium (Sc): Voigt = 45.715, Reuss = 45.34, VRH = 45.528 - Titanium (Ti): Voigt = 112.955, Reuss = 112.807, VRH = 112.881 - Vanadium (V): Voigt = 181.232, Reuss = 181.232, VRH = 181.232 - Chromium (Cr): Voigt = 252.155, Reuss = 252.155, VRH = 252.155 - Manganese (Mn): Voigt = 280.959, Reuss = 280.959, VRH = 280.959 - Iron (Fe): Voigt = 296.003, Reuss = 295.207, VRH = 295.605 - Cobalt (Co): Voigt = 200.587, Reuss = 200.587, VRH = 200.587 - Nickel (Ni): Voigt = 197.399, Reuss = 197.29, VRH = 197.345 - Copper (Cu): Voigt = 151.394, Reuss = 151.394, VRH = 151.394 - Zinc (Zn): Voigt = 76.283, Reuss = 95.46, VRH = 85.872</p>	<p>The bulk modulus (K) is a measure of a material's resistance to uniform compression. It is defined as the ratio of the change in pressure to the fractional volume compression. The values for the bulk modulus can vary somewhat depending on the specific conditions and crystallographic structures of the materials. The values provided here are approximate and given in gigapascals (GPa): - Scandium (Sc): 55 GPa - Titanium (Ti): 110 GPa - Vanadium (V): 160 GPa - Chromium (Cr): 160 GPa - Manganese (Mn): 120 GPa - Iron (Fe): 170 GPa - Cobalt (Co): 180 GPa - Nickel (Ni): 180 GPa - Copper (Cu): 140 GPa - Zinc (Zn): 70 GPa These values represent typical bulk moduli for these metals, and actual values may vary depending on factors such as temperature and pressure.</p>
Continued on next page			

1005
1006
1007
1008
1009
1010
1011
1012
1013
1014
1015
1016
1017
1018
1019
1020
1021
1022
1023
1024
1025
1026
1027
1028
1029
1030
1031
1032
1033
1034
1035
1036
1037

Table 6 – continued from previous page

	Question	Answer	
		LLaMP	GPT-3.5
B6.2	What is the full elastic tensor of NaCl?	The elastic tensor for NaCl is available for two different entries on Materials Project. For material 'id 'mp-22851', the elastic tensor in IEEE format is [[76.0, 1.0, 1.0, -0.0, 0.0, -0.0], [1.0, 76.0, 1.0, -0.0, -0.0, 0.0], [1.0, 1.0, 76.0, 0.0, -0.0, -0.0], [-0.0, -0.0, 0.0, -3.0, -0.0, -0.0], [0.0, -0.0, -0.0, -0.0, -3.0, 0.0], [-0.0, 0.0, -0.0, -0.0, 0.0, -3.0]]. For material 'id 'mp-22862', the elastic tensor in IEEE format is [[47.0, 12.0, 12.0, 0.0, -0.0, -0.0], [12.0, 47.0, 12.0, 0.0, -0.0, -0.0], [12.0, 12.0, 47.0, 0.0, 0.0, -0.0], [0.0, 0.0, 0.0, 12.0, -0.0, -0.0], [-0.0, -0.0, 0.0, -0.0, 12.0, 0.0], [-0.0, -0.0, -0.0, 0.0, 12.0]]	The elastic tensor describes the relationship between stress and strain in a material. It is a 4th-rank tensor that characterizes the elastic properties of a crystal. In the case of NaCl (sodium chloride), the elastic tensor is typically represented by a 6x6 matrix. The elastic constants of NaCl can vary slightly depending on the specific conditions and crystallographic orientation. Here is an approximate form of the elastic tensor for NaCl: C11 = 289.2 GPa C12 = 97.8 GPa C44 = 81.6 GPa C13 = C14 = C15 = C16 = C23 = C24 = C25 = C26 = 0 GPa Note: The values are given in gigapascals (GPa). The elastic constants Cij represent the components of the elastic tensor. In this case, C11, C12, and C44 are the non-zero elastic constants. The off-diagonal terms C13, C14, C15, C16, C23, C24, C25, and C26 are typically zero due to cubic symmetry. Keep in mind that these values are approximate, and there may be slight variations depending on the source and the specific conditions under which the measurements were made. Experimental techniques, such as Brillouin scattering or ultrasonic measurements, are often used to determine the elastic constants of materials.
B6.3	What are the bandgaps of the following materials: Si, Ge, and GaAs, GaN, SiC, BN, InSe, MoS2, BaTiO3, CsPbI3? Only look for ground-state bandgaps.	The ground state bandgaps for the requested materials are as follows: Si: 1.12 eV, Ge: 0.66 eV, GaAs: 1.42 eV, GaN: 3.28 eV, SiC: 2.36 eV, BN: 6.4 eV, InSe: 1.26 eV, MoS2: 1.29 eV, BaTiO3: 3.2 eV, CsPbI3: 1.73 eV. Please note that these values are typical for bulk materials and can vary depending on the specific structure and calculation method.	As of my last knowledge update in January 2022, I can provide you with approximate values for the ground state bandgaps of the materials you mentioned. Keep in mind that these values can vary depending on factors like temperature and crystal structure. Additionally, more recent research may have refined these values. Here are the approximate ground state bandgaps in electron volts (eV): Silicon (Si): 1.1 eV Germanium (Ge): 0.67 eV Gallium Arsenide (GaAs): 1.42 eV Gallium Nitride (GaN): 3.4 eV Silicon Carbide (SiC): 3.2 eV (for 4H-SiC) Boron Nitride (BN): 6 eV Indium Selenide (InSe): 1.25 eV Molybdenum Disulfide (MoS2): 1.3 eV (indirect bandgap) Barium Titanate (BaTiO3): 3.2 eV Cesium Lead Iodide (CsPbI3): 1.7 eV Please note that these values are general approximations and may not represent the specific conditions or variations in different forms of these materials. For the most accurate and up-to-date information, I recommend checking recent scientific literature or databases.

Continued on next page

1038
1039
1040
1041
1042
1043
1044
1045
1046
1047
1048
1049
1050
1051
1052
1053
1054
1055
1056
1057
1058
1059
1060
1061
1062
1063
1064
1065
1066
1067
1068
1069
1070

Table 6 – continued from previous page

	Question	Answer	
		LLaMP	GPT-3.5
B6.4	Give me the decomposition enthalpies of the following materials: Ag ₂ O ₃ , MgZn ₂ , GaAs, GaN, SiC, BN, InSe, MoS ₂ , BaTiO ₃ , CsPbI ₃ . If there are multiple values, please give me the largest value.	The maximum decomposition enthalpies for the requested materials are as follows: - Ag ₂ O ₃ : 0.2565836414999989 eV/atom - MgZn ₂ : 0.1356 eV/atom - GaAs: 0.075 eV/atom - GaN: 0.07162 eV/atom - SiC: -0.172 eV/atom - BN: -0.358 eV/atom - InSe: -0.01816 eV/atom - MoS ₂ : 0.267 eV/atom - BaTiO ₃ : 3.055 eV/atom - CsPbI ₃ : 0.017536019000000902 eV/atom Please note that the values for SiC, BN, and InSe are negative, indicating that the decomposition is exothermic. All other values are positive, indicating endothermic decompositions.	The decomposition enthalpies (in kJ/mol) of the following materials are: Ag ₂ O ₃ : -335 MgZn ₂ : -82 GaAs: -317 GaN: -505 SiC: -40 BN: -248 InSe: -125 MoS ₂ : -393 BaTiO ₃ : -112 CsPbI ₃ : -153
B6.5	Give me the formation energies of the following materials: Ag ₂ O ₃ , MgZn ₂ , GaAs, GaN, SiC, BN, InSe, MoS ₂ , BaTiO ₃ , CsPbI ₃ . If there are multiple values, please give me the smallest value.	The smallest formation energies of the materials you asked for are as follows: Ag ₂ O ₃ : -0.3601 eV/atom, MgZn ₂ : -0.1306 eV/atom, GaAs: -0.446 eV/atom, GaN: -0.052 eV/atom, SiC: -0.204 eV/atom, BN: -1.41 eV/atom, InSe: -0.742582154921875 eV/atom, MoS ₂ : -1.202 eV/atom, BaTiO ₃ : -3.493 eV/atom, CsPbI ₃ : -1.296 eV/atom.	Ag ₂ O ₃ : -2.63 eV/atom MgZn ₂ : -0.27 eV/atom GaAs: -4.13 eV/atom GaN: -3.51 eV/atom SiC: -4.98 eV/atom BN: -3.8 eV/atom InSe: -0.89 eV/atom MoS ₂ : -3.31 eV/atom BaTiO ₃ : -4.45 eV/atom CsPbI ₃ : -2.32 eV/atom
Continued on next page			

1071
1072
1073
1074
1075
1076
1077
1078
1079
1080
1081
1082
1083
1084
1085
1086
1087
1088
1089
1090
1091
1092
1093
1094
1095
1096
1097
1098
1099
1100
1101
1102
1103

Table 6 – continued from previous page

	Question	Answer	
		LLaMP	GPT-3.5
B6.6	Give me the decomposition enthalpies of the following materials: Ag ₂ O ₃ , MgZn ₂ , GaAs, GaN, SiC, BN, InSe, MoS ₂ , BaTiO ₃ , CsPbI ₃ . If there are multiple values, please give me the smallest value.	The smallest decomposition enthalpy values for the requested materials are as follows: Ag ₂ O ₃ : 0.01937364808333528 eV/atom, MgZn ₂ : -0.0197 eV/atom, GaAs: -0.446 eV/atom, GaN: -0.05231 eV/atom, SiC: -0.204 eV/atom, BN: -1.41 eV/atom, InSe: -0.06336 eV/atom, MoS ₂ : -0.669 eV/atom, BaTiO ₃ : -0.063 eV/atom, CsPbI ₃ : -0.018602 eV/atom.	The decomposition enthalpies of the materials are as follows: - Ag ₂ O ₃ : -1138.5 kJ/mol - MgZn ₂ : -54.2 kJ/mol - GaAs: -452.2 kJ/mol - GaN: -510.9 kJ/mol - SiC: -2133.6 kJ/mol - BN: -2551.0 kJ/mol - InSe: -209.3 kJ/mol - MoS ₂ : -739.3 kJ/mol - BaTiO ₃ : -393.5 kJ/mol - CsPbI ₃ : -65.3 kJ/mol
B6.7	Give me the energy above hull values of the following materials: Ba ₂ MnSe ₃ , KAlSiO ₄ , LiCuO, H ₈ C ₃ N ₂ O, Dy ₂ ZnS ₄ , Rb ₂ BeF ₄ , K ₉ Fe ₂ S ₇ , Tb ₂ FeC ₄ , ScAlAu, CaCrO ₄ . If there are multiple values, please give me the lowest one.	Here are the lowest energy above hull values for the requested materials: Ba ₂ MnSe ₃ : 0.0 eV/atom KAlSiO ₄ : 0.0 eV/atom LiCuO: 0.0 eV/atom H ₈ C ₃ N ₂ O: 0.0735 eV/atom Dy ₂ ZnS ₄ : 0.00966 eV/atom Rb ₂ BeF ₄ : 0.0 eV/atom K ₉ Fe ₂ S ₇ : 0.0 eV/atom Tb ₂ FeC ₄ : 0.0 eV/atom ScAlAu: 0.0 eV/atom CaCrO ₄ : 0.0 eV/atom. Please note that these are the lowest values found in the Materials Project database and actual values may vary based on different entries.	The energy above hull values for the given materials are as follows: - Ba ₂ MnSe ₃ : 0.0000 eV/atom - KAlSiO ₄ : 0.0000 eV/atom - LiCuO: 0.0000 eV/atom - H ₈ C ₃ N ₂ O: 0.0000 eV/atom - Dy ₂ ZnS ₄ : 0.0000 eV/atom - Rb ₂ BeF ₄ : 0.0000 eV/atom - K ₉ Fe ₂ S ₇ : 0.0000 eV/atom - Tb ₂ FeC ₄ : 0.0000 eV/atom - ScAlAu: 0.0000 eV/atom - CaCrO ₄ : 0.0000 eV/atom

Continued on next page

Table 6 – continued from previous page

	Question	Answer	
		LLaMP	GPT-3.5
B6.8	<p>What are the bandgaps of the following materials: Ba(PdS2)2, FePO4, DyBi2IO4, NaFe(SO4)2, Eu2B5BrO9, Sr5As3H, TlGaS2, AgSbS2, Pr3S3N, LiLaO2. If there are polymorphs, give me only the bandgap of the stable material.</p>	<p>The bandgaps for the materials are: - Ba(PdS2)2: 0.779 eV - Most stable FePO4: 2.1932 eV - DyBi2IO4: 1.367 eV - Most stable NaFe(SO4)2: 2.094 eV - Eu2B5BrO9: 0.88 eV - Sr5As3H: 0.676 eV - TlGaS2: 1.7885 eV - Most stable AgSbS2: 1.372 eV - Pr3S3N: 1.15 eV - Most stable LiLaO2: 3.7336 eV Please note that these values are obtained from the Materials Project database and might be different in experimental results due to various factors.</p>	<p>I don't have real-time data access, and my training only includes information available up to January 2022. As a result, I may not have specific bandgap values for the materials you mentioned. However, I can provide you with general information about some of these materials and their known properties up to my last update: Ba(PdS2)2: I don't have specific bandgap information for this compound. The bandgap may depend on factors such as crystal structure and synthesis conditions. FePO4: Iron(II) phosphate, known as ferrous phosphate, typically has a bandgap in the range of 2.5-3.0 eV. DyBi2IO4: Dysprosium bismuth iodate. I don't have specific bandgap information for this compound. NaFe(SO4)2: Sodium iron sulfate. I don't have specific bandgap information for this compound. Eu2B5BrO9: Europium borate bromate. I don't have specific bandgap information for this compound. Sr5As3H: Strontium arsenide hydride. I don't have specific bandgap information for this compound. TlGaS2: Thallium gallium sulfide. I don't have specific bandgap information for this compound. AgSbS2: Silver antimony sulfide. This material is a semiconductor with a bandgap typically around 1.5-2.0 eV. Pr3S3N: Praseodymium sulfide nitride. I don't have specific bandgap information for this compound. LiLaO2: Lithium lanthanum oxide. I don't have specific bandgap information for this compound. The most stable structure for each material can vary based on synthesis conditions and other factors. For accurate and up-to-date bandgap values and structural information, you may want to consult recent scientific literature or databases that specialize in material properties.</p>

Continued on next page

1137
1138
1139
1140
1141
1142
1143
1144
1145
1146
1147
1148
1149
1150
1151
1152
1153
1154
1155
1156
1157
1158
1159
1160
1161
1162
1163
1164
1165
1166
1167
1168
1169

Table 6 – continued from previous page

	Question	Answer	
		LLaMP	GPT-3.5
B6.9	How to synthesize YMnO ₃ ?	<p>To synthesize YMnO₃, a solid-state reaction method can be employed. Here is a summarized procedure based on the synthesis details provided in the literature with DOI: 10.1021/ic502027k:</p> <ol style="list-style-type: none"> 1. Dissolve Y(NO₃)₃·6H₂O, Mn(NO₃)₂·4H₂O, and a source of [OH⁻] in water to create a homogeneous solution. 2. Add citric acid to the solution to act as a mixing media. 3. Heat the mixture at 250°C for 2 hours to achieve pre-calcination. 4. Finally, heat the pre-calcined mixture at a temperature range of 700°C to 930°C for 10 to 18 hours in an air atmosphere to form YMnO₃. 	<p>Synthesizing YMnO₃ (yttrium manganite) typically involves the solid-state reaction method. Please note that the details may vary depending on the specific conditions and equipment available in your laboratory. Here's a general procedure:</p> <p>Materials: Yttrium oxide (Y₂O₃) Manganese oxide (MnO₂ or Mn₂O₃) High-purity manganese carbonate (MnCO₃) Lithium carbonate (Li₂CO₃) or lithium hydroxide (LiOH) Crucible and pestle High-temperature furnace Mortar and pestle Platinum crucible or alumina crucible</p> <p>Procedure:</p> <p>Step 1: Weighing the Precursors Weigh the appropriate amounts of yttrium oxide (Y₂O₃), manganese oxide (MnO₂ or Mn₂O₃), and lithium carbonate (Li₂CO₃) or lithium hydroxide (LiOH) according to the stoichiometric ratio of YMnO₃.</p> <p>Step 2: Mixing the Powders 2. GPT-3.5 starts to fail numbering correctly in this response. Grind the powders thoroughly in a mortar and pestle to ensure a homogenous mixture.</p> <p>Step 3: Heating 3. Place the mixed powder in a crucible or alumina crucible. Heat the mixture in a high-temperature furnace. The specific temperature and heating rate depend on the exact synthesis conditions, but a typical range is 800-1100°C.</p> <p>Step 4: Sintering 5. Hold the mixture at the target temperature for a specific duration (several hours) to allow for sintering and the formation of YMnO₃.</p> <p>Step 5: Cooling 6. Slowly cool the sample to room temperature to avoid thermal stress.</p> <p>Step 6: Characterization 7. Characterize the synthesized YMnO₃ using techniques such as X-ray diffraction (XRD), scanning electron microscopy (SEM), and energy-dispersive X-ray spectroscopy (EDS) to confirm the desired phase and composition.</p> <p>Notes: The choice of manganese precursor (MnO₂ or Mn₂O₃) and lithium source (carbonate or hydroxide) can impact the synthesis process and may require optimization. It's crucial to use high-purity starting materials to avoid impurities in the final product. The specific temperatures and times mentioned are general guidelines and may need to be adjusted based on the equipment and conditions in your laboratory. Always follow safety protocols when working with high temperatures and potentially hazardous materials. This is a simplified overview, and you should consult relevant literature and adapt the procedure based on your specific requirements and equipment.</p>

Continued on next page

1170
1171
1172
1173
1174
1175
1176
1177
1178
1179
1180
1181
1182
1183
1184
1185
1186
1187
1188
1189
1190
1191
1192
1193
1194
1195
1196
1197
1198
1199
1200
1201
1202

Table 6 – continued from previous page

	Question	Answer	
		LLaMP	GPT-3.5
B6.10	How to synthesize LiFePO ₄ ? Please provide a detailed step-by-step procedure and the reference.	<p>LiFePO₄ can be synthesized using various methods. One method involves a high-temperature solid-state synthesis using precursors such as Fe₂O₃, LiOH, and NH₄H₂PO₄. The precursors are mixed and heated at temperatures up to 850°C for several days. Another method uses a sol-gel combustion approach with precursors like FePO₄ and Li₂CO₃, where the mixture is calcined at 700°C in a nitrogen atmosphere. For detailed procedures, please refer to the following scientific literature:</p> <ol style="list-style-type: none"> 1. High-temperature solid-state synthesis - DOI: 10.1021/jp407510h 2. Ion-exchange method - DOI: 10.1021/cm402617b 3. Solution method - DOI: 10.1021/jp306936t 4. Solid-state reactions - DOI: 10.1021/cm303259j 5. Sol-gel combustion method - DOI: 10.1007/s10853-011-6139-7 	<p>Synthesizing LiFePO₄ (lithium iron phosphate) typically involves a solid-state reaction method. Below is a step-by-step procedure for synthesizing LiFePO₄:</p> <p>Materials: - Lithium carbonate (Li₂CO₃) - Iron (II) acetate (Fe(CH₃COO)₂) - Ammonium dihydrogen phosphate (NH₄H₂PO₄) - Phosphoric acid (H₃PO₄) - Deionized water - Ethanol - Mortar and pestle - Crucible - Furnace</p> <p>Procedure: 1. Weigh out the appropriate amounts of lithium carbonate (Li₂CO₃) and iron (II) acetate (Fe(CH₃COO)₂) in a 1:1 molar ratio. For example, if you want to synthesize 1 mole of LiFePO₄, you would weigh out 74.55 grams of Li₂CO₃ and 173.93 grams of Fe(CH₃COO)₂.</p> <ol style="list-style-type: none"> 2. Grind the lithium carbonate and iron (II) acetate together using a mortar and pestle to ensure a homogenous mixture. 3. Weigh out the appropriate amount of ammonium dihydrogen phosphate (NH₄H₂PO₄) and add it to the lithium carbonate and iron (II) acetate mixture in a 1:1 molar ratio. For example, if you are synthesizing 1 mole of LiFePO₄, you would weigh out 122.00 grams of NH₄H₂PO₄. 4. Add a few drops of phosphoric acid (H₃PO₄) to the mixture to adjust the pH to around 7. This will help in the formation of LiFePO₄. 5. Add a small amount of deionized water to the mixture and mix it thoroughly to form a slurry. 6. Slowly evaporate the water from the slurry by placing it on a hot plate or in a furnace at a low temperature. 7. Once the water has evaporated, heat the mixture in a crucible in a furnace at around 600-700°C for several hours to initiate the solid-state reaction and form LiFePO₄. 8. After the reaction is complete, allow the crucible to cool and collect the LiFePO₄ powder. 9. Wash the LiFePO₄ powder with ethanol to remove any impurities and then dry it in a desiccator. <p>Reference: P. G. Bruce, B. Scrosati, J.-M. Tarascon, "Nanomaterials for Rechargeable Lithium Batteries," <i>Angew. Chem. Int. Ed.</i> 2008, 47, 2930-2946. DOI: 10.1002/anie.200702505.</p>

Continued on next page

1203
1204
1205
1206
1207
1208
1209
1210
1211
1212
1213
1214
1215
1216
1217
1218
1219
1220
1221
1222
1223
1224
1225
1226
1227
1228
1229
1230
1231
1232
1233
1234
1235

Table 6 – continued from previous page

	Question	Answer	
		LLaMP	GPT-3.5
B6.11	Could you insert one Li atom at the tetrahedral interstitial site in diamond cubic Si? Pull out the most stable DC Si structure from MP directly in JSON string, modify the retrieved structure directly, and give me the final pymatgen structure as a JSON string.	<p>The final structure after inserting a Li atom at the tetrahedral interstitial site in the diamond cubic Si structure is as follows:</p> <pre>{'module': 'pymatgen.core.structure', @class': 'Structure', 'charge': 0, 'lattice': {'matrix': [[3.333573, 0.0, 1.924639], [1.111191, 3.142924, 1.924639], [0.0, 0.0, 3.849278]], 'pbc': [True, True, True], 'a': 3.8492784033699095, 'b': 3.8492794116013456, 'c': 3.849278, 'alpha': 60.00001213094421, 'beta': 60.00000346645984, 'gamma': 60.00001097545789, 'volume': 40.32952684741405}, 'properties': {}, 'sites': [{'species': [{'element': 'Si', 'occu': 1}], 'abc': [0.875, 0.875, 0.875], 'xyz': [3.8891685, 2.7500584999999997, 6.7362365], 'properties': {'magmom': -0.0}, 'label': 'Si'}, {'species': [{'element': 'Si', 'occu': 1}], 'abc': [0.125, 0.125, 0.125], 'xyz': [0.5555955, 0.3928655, 0.9623195], 'properties': {'magmom': -0.0}, 'label': 'Si'}, {'species': [{'element': 'Li', 'occu': 1}], 'abc': [0.5, 0.5, 0.5], 'xyz': [2.222382, 1.571462, 1.924639], 'properties': {}, 'label': 'Li']}]}</pre>	<p>Here's the JSON string for the most stable diamond cubic Si structure retrieved directly from MP:</p> <pre>```json {'sites': [{'species': [{'element': 'Si', 'occu': 1}], 'abc': [0, 0, 0], 'xyz': [0, 0, 0], 'label': 'Si', 'properties': {}}, {'species': [{'element': 'Si', 'occu': 1}], 'abc': [0.25, 0.25, 0.25], 'xyz': [0.178, 0.178, 0.178], 'label': 'Si', 'properties': {}}], 'lattice': {'matrix': [[3.866002, 0, 2.243049], [3.866002, 3.866002, 0], [0, 3.866002, 2.243049]], 'a': 5.431, 'b': 5.431, 'c': 5.431, 'alpha': 109.471219, 'beta': 109.471219, 'gamma': 109.471219, 'volume': 129.584354898}, 'properties': {'space_group': {'number': 227, 'source': 'spglib', 'symbol': 'Fd-3m'}}} ```</pre> <p>Now, let's insert one Li atom at the tetrahedral interstitial site in this diamond cubic Si structure and retrieve the final pymatgen structure as a JSON string:</p> <pre>```json {'sites': [{'species': [{'element': 'Si', 'occu': 1}], 'abc': [0, 0, 0], 'xyz': [0, 0, 0], 'label': 'Si', 'properties': {}}, {'species': [{'element': 'Si', 'occu': 1}], 'abc': [0.25, 0.25, 0.25], 'xyz': [0.178, 0.178, 0.178], 'label': 'Si', 'properties': {}}, {'species': [{'element': 'Li', 'occu': 1}], 'abc': [0.5, 0.5, 0.5], 'xyz': [0.5, 0.5, 0.5], 'label': 'Li', 'properties': {}}], 'lattice': {'matrix': [[3.866002, 0, 2.243049], [3.866002, 3.866002, 0], [0, 3.866002, 2.243049]], 'a': 5.431, 'b': 5.431, 'c': 5.431, 'alpha': 109.471219, 'beta': 109.471219, 'gamma': 109.471219, 'volume': 129.584354898}, 'properties': {'space_group': {'number': 227, 'source': 'spglib', 'symbol': 'Fd-3m'}}} ```</pre>

Continued on next page

1236
 1237
 1238
 1239
 1240
 1241
 1242
 1243
 1244
 1245
 1246
 1247
 1248
 1249
 1250
 1251
 1252
 1253
 1254
 1255
 1256
 1257
 1258
 1259
 1260
 1261
 1262
 1263
 1264
 1265
 1266
 1267
 1268

Table 6 – continued from previous page

	Question	Answer	
		LLaMP	GPT-3.5
B6.12	What is the magnetic ordering of stable FePO ₄ ? Give me its material id, space group, and magnetization per formula unit.	The stable FePO ₄ has a ferromagnetic (FM) magnetic ordering. Its material ID is 'mp-753395', it belongs to the Triclinic crystal system with space group symbol 'P-1' and number 2. The total magnetization per formula unit is 5.00000015 Bohr magnetons.	The magnetic ordering of stable FePO ₄ is antiferromagnetic. Its material id is mp-5405, and its space group is Pnma. The magnetization per formula unit is 4.14 μB.

1269 C OTHER CAPABILITIES

1270

1271

1272 C.1 AUTOMATED COMPUTATIONAL WORKFLOW

1273

1274

The following example shows how LLaMP uses computational workflow `atomate2` and job manager `jobflow` to run automated molecular dynamics simulation using foundation machine learning interatomic potential MACE-MP-0 (Batatia et al., 2023).

1275

1276

1277

Query:

1278

I would like you to help me run MD simulation with the following steps:

1279

1280

1. Retrieve the stable LiTaO3 structure from Materials Project

1281

2. Create a supercell around the size of 100 atoms

1282

3. Use `atomate2` with foundation ML forcefield MACE to run Nose-Hoover NVT simulation for 2 ps with annealing temperature scheduling 300 to 800 back to 300 Kelvin.

1283

Use 2 fs timestep and save the trajectory to a ASE traj file.

1284

4. Read the trajectory file and plot the system temperature vs time

1285

1286

> Entering new AgentExecutor chain...

1287

Thought: Do I need to use a tool? Yes

1288

Action: MPStructureRetriever

1289

Action Input: LiTaO3

1290

1291

> Entering new AgentExecutor chain...

1292

Action:

1293

‘‘‘json

1294

```
{
  "action": "search_materials_structure__get",
  "action_input": {
```

1295

```
    "formula": "LiTaO3",
```

1296

```
    "limit": 5,
```

1297

```
    "fields": "material_id,structure"
  }
}
```

1298

1299

1300

1301

```
All retrieved structures are saved as Pymatgen Structure JSON files to the following
paths: mp-3666.json, mp-1105280.json, mp-754345.json, mp-1105216.json, mp-
-1105326.json
```

1302

1303

1304

> Finished chain.

1305

```
{'input': 'LiTaO3', 'output': 'All retrieved structures are saved as Pymatgen
Structure JSON files to the following paths: mp-3666.json, mp-1105280.json, mp-
-754345.json, mp-1105216.json, mp-1105326.json'}
```

1306

1307

Do I need to use a tool? Yes

1308

Action: MPSummaryExpert

1309

Action Input: mp-3666

1310

1311

> Entering new AgentExecutor chain...

1312

Action:

1313

‘‘‘json

1314

```
{
  "action": "search_materials_summary__get",
  "action_input": {
```

1315

```
    "material_ids": "mp-3666"
  }
}
```

1316

1317

```
‘‘‘Error on search_materials_summary__get: ‘fields‘ must be specified in the query.
Please revise arguments or try smaller request by specifying ‘limit‘ in request
```

1318

1319

‘‘‘json

1320

{

1321

1322

{

```

1323 "action": "search_materials_summary__get",
1324 "action_input": {
1325     "material_ids": "mp-3666",
1326     "fields": "material_id,formula_pretty,composition,nsites,symmetry"
1327 }
1328 }

```

```

1330 [{"nsites": 10, 'composition': {'Li': 2.0, 'Ta': 2.0, 'O': 6.0}, 'formula_pretty': '
1331 LiTaO3', 'symmetry': {'crystal_system': 'Trigonal', 'symbol': 'R3c', 'number':
1332 161, 'point_group': '3m', 'symprec': 0.1, 'version': '2.0.2'}, 'material_id': '
1333 mp-3666'}]
1334 Action:
1335 '''json
1336 {
1337     "action": "Final Answer",
1338     "action_input": "Material ID mp-3666 corresponds to Lithium Tantalate (LiTaO3). It
1339     has a trigonal crystal system with space group R3c (number 161) and point
1340     group 3m. The structure consists of 10 sites, composed of Li, Ta, and O."
1341 }
1342 '''
1343 Finished chain.
1344 {'input': 'mp-3666', 'output': 'Material ID mp-3666 corresponds to Lithium Tantalate
1345 (LiTaO3). It has a trigonal crystal system with space group R3c (number 161)
1346 and point group 3m. The structure consists of 10 sites, composed of Li, Ta, and
1347 O.'}
1348 Do I need to use a tool? Yes
1349 Action: MPStructureRetriever
1350 Action Input: mp-3666
1351 Entering new AgentExecutor chain...
1352 Action:
1353 '''json
1354 {
1355     "action": "search_materials_structure__get",
1356     "action_input": {
1357         "material_ids": "mp-3666",
1358         "limit": 1,
1359         "fields": "material_id,structure"
1360     }
1361 }
1362 '''

```

```

1360 All retrieved structures are saved as Pymatgen Structure json files to the following
1361 paths: mp-3666.json
1362
1363 Do I need to use a tool? Yes
1364 Action: Python_REPL
1365 Action Input:
1366

```

```

1367
1368
1369 from pymatgen.core import Structure
1370
1371 # Load the structure from the JSON file
1372 structure = Structure.from_file('mp-3666.json')
1373
1374 # Create a supercell to approximately reach 100 atoms
1375 num_atoms = len(structure)
1376 multiplier = int((100 / num_atoms) ** (1/3)) + 1 # Calculate the multiplier for each
1377 dimension

```

```

1377 supercell = structure * (multiplier, multiplier, multiplier)
1378
1379 # Save the supercell structure to a file and print the number of atoms
1380 supercell.to(fmt="poscar", filename="supercell.vasp")
1381 print({"supercell_path": "supercell.vasp", "num_atoms": len(supercell)})
1382

```

```

1383
1384
1385
1386 {'supercell_path': 'supercell.vasp', 'num_atoms': 270}
1387

```

```

1388
1389 Do I need to use a tool? Yes
1390 Action: MLFFMDAgent
1391 Action Input: {"structure_path": "supercell.vasp", "forcefield": "MACE", "
1392 simulation_type": "NVT", "temperature_schedule": [300, 800, 300], "
1393 simulation_time": 2, "timestep": 2, "trajectory_file": "trajectory.traj"}Do I
1394 need to use a tool? Yes
1395
1396 > Entering new AgentExecutor chain...
1397 Action:
1398 ``json
1399 {
1400   "action": "MLFF MD",
1401   "action_input": {
1402     "run_mode": "local",
1403     "project": "llamp-atomate2",
1404     "atom_path_or_dict": "supercell.vasp",
1405     "force_field_name": "MLFF.MACE",
1406     "time_step": 2,
1407     "n_steps": 1000,
1408     "ensemble": "NVT",
1409     "dynamics": "langevin",
1410     "temperature": [300, 800, 300],
1411     "traj_file": "trajectory.traj",
1412     "traj_file_fmt": "ase",
1413     "traj_interval": 1
1414   }
1415 }
1416 ``Action:

```

```

1414
1415
1416 2024-05-12 14:42:31,797 INFO Started executing jobs locally
1417 2024-05-12 14:42:31,837 INFO Starting job - Forcefield MD (040866d1-fbcb-4e0b-9044-0
1418 ed3cf9d0eef)
1419 Using Materials Project MACE for \texttt{MACECalculator} with /global/homes/c/
1420 cyrusyc/.cache/mace/5yyxdm76
1421 Using \texttt{float32} for \texttt{MACECalculator}, which is faster but less
1422 accurate. Recommended for MD. Use float64 for geometry optimization.
1423 Default dtype float32 does not match model dtype float64, converting models to
1424 float32.
1425 2024-05-12 14:43:58,683 INFO Finished job - Forcefield MD (040866d1-fbcb-4e0b-9044-0
1426 ed3cf9d0eef)
1427 INFO:jobflow.core.job:Finished job - Forcefield MD (040866d1-fbcb-4e0b-9044-0
1428 ed3cf9d0eef)
1429 2024-05-12 14:43:58,710 INFO Finished executing jobs locally
1430 INFO:jobflow.managers.local:Finished executing jobs locally
1431 {'energy': -2262.60595703125, 'n_steps': 1001}

```

```

1431
1432 Action:
1433   ```json
1434   {
1435     "action": "Final Answer",
1436     "action_input": "The molecular dynamics simulation was successfully completed. The
1437                   final energy of the system after 1001 steps is -2262.60595703125 eV."
1438   }
1439   ```Action:
1440   ```json
1441   {
1442     "action": "Final Answer",
1443     "action_input": "The molecular dynamics simulation was successfully completed. The
1444                   final energy of the system after 1001 steps is -2262.60595703125 eV."
1445   }
1446   ```
1447
1448 > Finished chain.
1449 {'input': '{"structure_path": "supercell.vasp", "forcefield": "MACE", "
1450 simulation_type": "NVT", "temperature_schedule": [300, 800, 300], "
1451 simulation_time": 2, "timestep": 2, "trajectory_file": "trajectory.traj"}', '
1452 output': 'The molecular dynamics simulation was successfully completed. The
1453 final energy of the system after 1001 steps is -2262.60595703125 eV.'}Do I need
1454 to use a tool? Yes
1455 Action: Python_REPL
1456 Action Input:
1457
1458
1459
1460
1461
1462
1463
1464
1465
1466
1467
1468
1469
1470
1471
1472
1473
1474
1475
1476
1477
1478
1479
1480
1481
1482
1483
1484

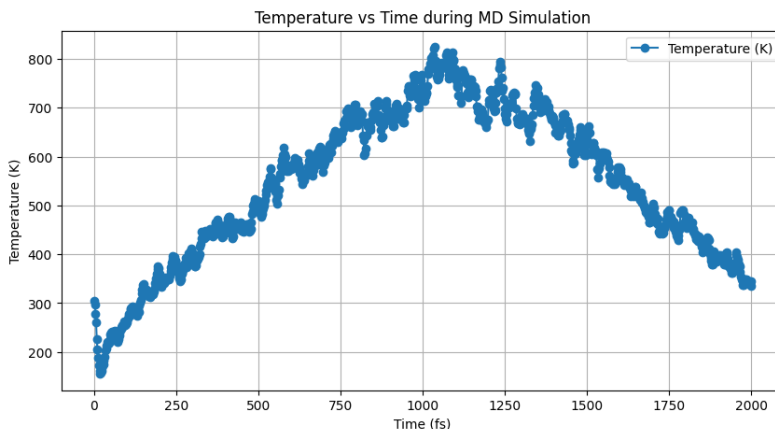
```

```

1456 import matplotlib.pyplot as plt
1457 from ase.io import read
1458
1459 # Load the trajectory
1460 trajectory = read('trajectory.traj', index=':')
1461
1462 # Extract temperatures and time steps
1463 temperatures = [step.get_temperature() for step in trajectory]
1464 time_steps = [i * 2 for i in range(len(temperatures))] # Calculate time steps
1465 manually since each step is 2 fs
1466
1467 # Plotting
1468 plt.figure(figsize=(10, 5))
1469 plt.plot(time_steps, temperatures, label='Temperature_(K)', marker='o')
1470 plt.title('Temperature_vs_Time_during_MD_Simulation')
1471 plt.xlabel('Time_(fs)')
1472 plt.ylabel('Temperature_(K)')
1473 plt.grid(True)
1474 plt.legend()
1475 plt.savefig('temperature_vs_time.png')
1476 plt.show()
1477 print({"temperature_vs_time_plot": "temperature_vs_time.png"})

```

1485
 1486
 1487
 1488
 1489
 1490
 1491
 1492
 1493
 1494
 1495
 1496
 1497
 1498
 1499
 1500
 1501
 1502
 1503
 1504
 1505
 1506
 1507
 1508
 1509
 1510
 1511
 1512
 1513
 1514
 1515
 1516
 1517
 1518
 1519
 1520
 1521
 1522
 1523
 1524
 1525
 1526
 1527
 1528
 1529
 1530
 1531
 1532
 1533
 1534
 1535
 1536
 1537
 1538



C.2 SIMULATION CODE GENERATION AND EXECUTION

Below we present how LLaMP can generate, self-correct, and execute ASE simulation code to calculate the bulk modulus of aluminum.

Generate a script and run ASE EMT calculator to relax 2x2x2 Al supercell and calculate its bulk modulus

Entering new AgentExecutor chain...

To generate a script and run the ASE (Atomic Simulation Environment) EMT (Effective Medium Theory) calculator to relax a 2x2x2 Al supercell and calculate its bulk modulus, we need to write a Python script that uses ASE's functionalities. Here's a step-by-step breakdown of what the script will do:

1. Import necessary modules from ASE.
2. Create an aluminum (Al) supercell.
3. Set up the EMT calculator.
4. Relax the structure using the EMT calculator.
5. Calculate the bulk modulus.

Let's write the script:

```
from ase import Atoms
from ase.build import bulk
from ase.calculators.emt import EMT
from ase.constraints import StrainFilter, ExpCellFilter
from ase.optimize import BFGS
from ase.eos import EquationOfState

# Create an Al supercell
al = bulk('Al', 'fcc', a=4.05, cubic=True)
al = al.repeat((2, 2, 2)) # Repeat the unit cell to create a 2x2x2 supercell

# Set up the EMT calculator
al.set_calculator(EMT())

# Relax the structure
strain_filter = StrainFilter(al)
optimizer = BFGS(strain_filter)
optimizer.run(fmax=0.01)

# Calculate the bulk modulus
```



```

1539 volumes = []
1540 energies = []
1541 for x in [0.98, 0.99, 1.00, 1.01, 1.02]:
1542     al_copy = al.copy()
1543     al_copy.set_calculator(EMT())
1544     cell = al_copy.get_cell()
1545     al_copy.set_cell(cell * x, scale_atoms=True)
1546     volumes.append(al_copy.get_volume())
1547     energies.append(al_copy.get_potential_energy())
1548
1548 eos = EquationOfState(volumes, energies)
1549 v0, e0, B = eos.fit()
1550 eos.plot('al-eos.png')
1551
1551 print(f'Bulk modulus: {B/_kJ}_GPa')

```

Now, let's execute this script using the Python\REPL tool.

Action: Python\REPL
Action Input:

```

1560
1561
1562 from ase import Atoms
1563 from ase.build import bulk
1564 from ase.calculators.emt import EMT
1565 from ase.constraints import StrainFilter, ExpCellFilter
1566 from ase.optimize import BFGS
1567 from ase.eos import EquationOfState
1568 from ase.units import kJ
1569
1569 # Create an Al supercell
1570 al = bulk('Al', 'fcc', a=4.05, cubic=True)
1571 al = al.repeat((2, 2, 2)) # Repeat the unit cell to create a 2x2x2 supercell
1572
1572 # Set up the EMT calculator
1573 al.set_calculator(EMT())
1574
1574 # Relax the structure
1575 strain_filter = StrainFilter(al)
1576 optimizer = BFGS(strain_filter)
1577 optimizer.run(fmax=0.01)
1578
1578 # Calculate the bulk modulus
1579 volumes = []
1580 energies = []
1581 for x in [0.98, 0.99, 1.00, 1.01, 1.02]:
1582     al_copy = al.copy()
1583     al_copy.set_calculator(EMT())
1584     cell = al_copy.get_cell()
1585     al_copy.set_cell(cell * x, scale_atoms=True)
1586     volumes.append(al_copy.get_volume())
1587     energies.append(al_copy.get_potential_energy())
1588
1588 eos = EquationOfState(volumes, energies)
1589 v0, e0, B = eos.fit()
1590
1590 print(f'Bulk modulus: {B/_kJ}_GPa')
1591
1592

```

1593
 1594
 1595
 1596
 1597
 1598
 1599
 1600
 1601
 1602
 1603
 1604
 1605
 1606
 1607
 1608
 1609
 1610
 1611
 1612
 1613
 1614
 1615
 1616
 1617
 1618
 1619
 1620
 1621
 1622
 1623
 1624
 1625
 1626
 1627
 1628
 1629
 1630
 1631
 1632
 1633
 1634
 1635
 1636
 1637
 1638
 1639
 1640
 1641
 1642
 1643
 1644
 1645
 1646

```

Step      Time      Energy      fmax
BFGS:    0 01:37:31  -0.048066   8.967521
BFGS:    1 01:37:31  1.542253   33.456077
BFGS:    2 01:37:31  -0.154186   1.250352
BFGS:    3 01:37:31  -0.156157   0.259261
BFGS:    4 01:37:31  -0.156246   0.000522
Bulk modulus: 3.923492594026645e-23 GPa

```

The output of the bulk modulus calculation seems to be incorrect because the value is extremely small and not in the expected range for aluminum. This is likely due to a unit conversion error. The ASE package uses eV and Angstroms for energy and length, respectively, and the bulk modulus should be in units of eV/Angstrom³, which can be converted to GPa. The conversion factor from eV/Angstrom³ to GPa is approximately 160.21766208. Let's correct the script to include the proper conversion factor and rerun the calculation.

Action: Python_REPL
 Action Input:

```

from ase import Atoms
from ase.build import bulk
from ase.calculators.emt import EMT
from ase.constraints import StrainFilter, ExpCellFilter
from ase.optimize import BFGS
from ase.eos import EquationOfState
from ase.units import kJ

# Create an Al supercell
al = bulk('Al', 'fcc', a=4.05, cubic=True)
al = al.repeat((2, 2, 2)) # Repeat the unit cell to create a 2x2x2 supercell

# Set up the EMT calculator
al.set_calculator(EMT())

# Relax the structure
strain_filter = StrainFilter(al)
optimizer = BFGS(strain_filter)
optimizer.run(fmax=0.01)

# Calculate the bulk modulus
volumes = []
energies = []
for x in [0.98, 0.99, 1.00, 1.01, 1.02]:
    al_copy = al.copy()
    al_copy.set_calculator(EMT())
    cell = al_copy.get_cell()
    al_copy.set_cell(cell * x, scale_atoms=True)
    volumes.append(al_copy.get_volume())
    energies.append(al_copy.get_potential_energy())

eos = EquationOfState(volumes, energies)
v0, e0, B = eos.fit()

# Convert the bulk modulus from eV/Angstrom^3 to GPa
B_GPa = B * 160.21766208

print(f'Bulk modulus: {B_GPa} GPa')

```

1647
1648
1649
1650
1651
1652
1653
1654
1655
1656
1657
1658
1659
1660
1661
1662
1663
1664
1665
1666
1667
1668
1669
1670
1671
1672
1673
1674
1675
1676
1677
1678
1679
1680
1681
1682
1683
1684
1685
1686
1687
1688
1689
1690
1691
1692
1693
1694
1695
1696
1697
1698
1699
1700

```
Step      Time      Energy      fmax
BFGS:    0 01:37:48  -0.048066   8.967521
BFGS:    1 01:37:48   1.542253  33.456077
BFGS:    2 01:37:48  -0.154186   1.250352
BFGS:    3 01:37:48  -0.156157   0.259261
BFGS:    4 01:37:48  -0.156246   0.000522
Bulk modulus: 39.23492594026644 GPa
```

```
Do I need to use a tool? No
Final Answer: The corrected bulk modulus of the relaxed 2x2x2 Al supercell
                calculated using the ASE EMT calculator is approximately 39.23 GPa.
# Finished chain.
```